Hindawi Publishing Corporation
Advances in Astronomy
Volume 2013, Article ID 390287, 25 pages
http://dx.doi.org/10.1155/2013/390287

Review Article

Anomalous Microwave Emission from Star Forming Regions

Anna M. M. Scaife

Physics & Astronomy, University of Southampton, Highfield, Southampton SO17 1BJ, UK

Correspondence should be addressed to Anna M. M. Scaife; a.scaife@soton.ac.uk

Received 7 June 2012; Accepted 11 January 2013

Academic Editor: Laurent Verstraete

The evidence for microwave emission from spinning dust grains has been strengthened considerably by its detection in a number of discrete astrophysical objects associated with star formation. These detections, in combination with statistical constraints on its presence on large angular scales in the diffuse ISM, have provided strong observational confirmation of an emission mechanism still referred to as anomalous. This emission has a peaked spectrum with a maximum in the microwave band; the present review discusses the continuum radio emission mechanisms which can contribute to this region of the electromagnetic spectrum, collects published results on the prevalence of anomalous microwave emission in a variety of star formation regions, presents the overall conclusions that may be drawn from the detections so far, and discusses the prospects for future research on the anomalous microwave emission attributed to spinning dust within star forming regions.

1. Introduction

The interstellar medium (ISM) of our galaxy and others is volume dominated by a small number of components. These components are differentiated by their temperature, ionization state, and density: the cold neutral medium (CNM) with hydrogen density $n_{\mathrm{H}} \approx 30\,\mathrm{cm}^{-3}$ and temperature 100 K, containing very little ionized material and no molecular gas; the warm neutral medium (WNM) with hydrogen density $n_{\mathrm{H}} \approx 0.3\,\mathrm{cm}^{-3}$ and temperatures of 5000–10^4 K, a low ionization fraction and no molecular component; the warm ionized medium (WIM), which has much in common with the WNM except that it is almost entirely ionized; as well as the low density hot ionized medium (HIM), with $n_{\mathrm{H}} \approx 0.001\,\mathrm{cm}^{-3}$ and temperatures of 10^6 K, which was first proposed by McKee and Ostriker ([1]; see also [2]) as the result of supernova shocks acting on the ambient ISM, and lead to the phrase "the violent ISM" being coined [3]. Between them these components make up three phases, where they exist with densities regulated by pressure equilibrium: the hot phase of the HIM, the cooler combined warm phase of the WIM and WNM, and the cold CNM phase [4].

In addition to these three phases there also exist quasistatic, long-lived components with pressures far in excess of the ambient ISM, which have a much smaller volume filling factor but represent the bulk of mass in the galaxy. These giant cloud components are virialized and gravitationally bound, and their increased pressure is a result of an ongoing internal struggle to produce pressure gradients which will balance their own self-gravity. Unlike the ambient ISM phases, these clouds are largely molecular with little ionized gas. Their high densities make them opaque to optical or ultraviolet radiation and they have very low temperatures of 10–30 K. These molecular clouds have a partly hierarchical structure, with a self-similar density structure thought to arise naturally from a turbulent medium [5]. Simulations of turbulent collapse have demonstrated that turbulent pressure in such regions can support the structure of a molecular cloud against collapse globally while still allowing local collapse to occur (e.g., [6]). It is this local collapse where (in the simplest picture) overdensities from fluctuations become unstable to gravity, which forms the even denser cores which collapse further to become stars. The largest of these structures, with masses in excess of $10^4\,\mathrm{M}_\odot$, are known as giant molecular clouds (GMCs). Within GMCs, individual overdensities are termed *clumps* and generally correspond to what are loosely termed *dark clouds* in the literature, with densities of 10^3–10^4 cm−3. These clouds do not necessarily go on to form stars, but can contain denser cores with $n_{\mathrm{H}} \approx 10^4$–$10^5\,\mathrm{cm}^{-3}$, and it is these cores that go on to form individual or multiple stars.

Once massive stars (typically O or B spectral type) have formed within these clouds, the effect of their energetic UV photon flux ($h\nu > 13.6\,eV$) on both their own surrounding cloud as well as those nearby is to cause photoionization of the molecular hydrogen to produce regions of fully ionized gas (HII regions). Those photons which escape the surrounding clouds completely travel further into the ISM to produce the warm ionized medium, which has similar temperatures to those of the HII regions ($\approx 10^4$ K). However, HII regions themselves have electron densities that range 1–10^5 cm^{-3}, far higher than those of the WIM. Consequently, with such high densities and large thermal velocities, these HII regions often cause otherwise collapsing clouds to expand into the ambient ISM, tearing apart the larger gravitationally bound molecular cloud.

It is these two higher pressure components of the ISM, molecular clouds, and HII regions which form the basis of this review. Such regions differ from the more diffuse medium where anomalous microwave emission was first detected by Leitch et al. [7] in the NCP. The unbound, low pressure gas of the NCP is often referred to as *cirrus* and may be considered to be composed of a combination of the ambient ISM constituents. Although the higher pressure components differ from this medium, the supposition that AME was related to the dust population presented a strong argument for examining these pre- and protostellar environments, where dust is expected to be ubiquitous.

In spite of the pervasive nature of dust in star formation regions, there is still debate about many of its properties. Dust is composed of carbonaceous, silicate, and/or metallic grains [8], but the actual mixture and structure are not well constrained. The shape of grains varies widely; they may be spherical, spheroidal, and fractal, or in the case of the very smallest grains they may be disk/sheet-like as expected for polycyclic aromatic hydrocarbons (PAHs; [9]) or needle-like [10]. Their sizes vary wildly, between a few tenths of a nanometre for the smallest grains which are expected to produce the anomalous microwave emission attributed to spinning dust, and several centimetres for the largest grains, or *pebbles*, found in the circumstellar/protoplanetary disks around young stars (e.g., [11]). Within cold molecular clouds the surface of these dust grains is expected to be coated by the depletion of molecules from the gas phase and, in the very coldest and densest regions, the formation of ice mantles [10]. All of these factors influence the observational parameters of the dust through their effects on emissivity and opacity as a function of wavelength, as well as the ratio of dust to gas which will vary between different environments [12].

Although star formation regions are generally studied at much shorter wavelengths, the identification of such regions with anomalous microwave emission attributed to spinning dust has led to a surge of observational studies at radio-microwave frequencies. These studies concentrate not only on small angular scales where radio emission is known historically to be associated with protostellar objects, but also on the extended scales of the clouds which contain this activity and indeed the wider complexes of such clouds.

The structure of this review is as follows: in Section 2, I give an overview of the radiation mechanisms contributing to the total microwave emission of star formation regions other than the anomalous microwave emission attributed to spinning dust; in Section 3, I discuss the possibilities for identifying spinning dust emission in star formation regions based on the theoretical predictions of Draine and Lazarian ([13]; hereafter DL98) and review the observational evidence in each case; in Section 4, I discuss the links to protostellar activity and the environmental conditions within star forming regions; in Section 5, I address the observational issues associated with the identification of the anomalous component; and in Section 6, I discuss the future observational prospects and possible directions for further study.

2. Radio Emission from Star Formation Regions

The mechanism and spectrum of the anomalous microwave emission from spinning dust are described elsewhere in this volume, and so I will not repeat that description here. However, at centimetre wavelengths, there are a number of alternative emission mechanisms which also contribute to the overall spectrum of star forming regions. The measured SED is consequently often a combination of multiple types of radiation processes and identifying the contribution from spinning dust alone requires careful separation of these components. Here I give a brief overview of the major alternative mechanisms which may be found to contribute to the overall spectrum. This overview is not an exhaustive description of these mechanisms, for which I refer the reader to the many more detailed investigations referenced in the text, but is intended to provide the reader with a working "toolkit" with which to understand and interpret the following discussions about the observational constraints on anomalous microwave emission from star formation regions.

Anomalous microwave emission is often discussed in the context of the three major radio emission mechanisms: synchrotron, bremsstrahlung, and thermal (i.e., vibrational) dust emission. Although such mechanisms are usually characterized by canonical spectral indices of $\alpha = -0.7, -0.1$, and $+3.8$, respectively (where $S_\nu \propto \nu^\alpha$), the detailed spectral dependencies of each vary substantially as a function of environment. Across the microwave band, broadly considered here as 1–100 GHz, the two dominant mechanisms will be thermal bremsstrahlung and thermal (i.e., vibrational) dust emission. As the separation of the anomalous microwave emission from other types of emission is highly important, I here briefly review these two major alternatives in the context of star forming regions.

2.1. Thermal Bremsstrahlung

2.1.1. General Principles. There is a variety of mechanisms expected to give rise to radio emission from star formation regions. The most commonly observed of these is that of thermal bremsstrahlung, or *free-free*, emission. This mechanism operates when charged particles, typically electrons, are accelerated by encountering another charged particle. Consequently radio free-free emission is expected to manifest from any environment populated by an ionized plasma. The

distribution and energy cutoff for scattering in such a plasma are characterized by the Gaunt factor, $\langle g_{\rm ff}\rangle$, which allows one to work out the (ratio of) absorption coefficient, κ_ν, for the plasma,

$$\kappa_\nu = 0.018 Z^2 N_e N_i T_e^{-3/2} \nu^2 \left\langle g_{\rm ff}\right\rangle . \quad (1)$$

Integration of this quantity along the line of sight, $\int \kappa_\nu {\rm d}\ell$, gives the optical path length (depth) for the free-free emission,

$$\tau_\nu = 3.014\times 10^{-2}\left(\frac{T_e}{\rm K}\right)^{-3/2}\left(\frac{\nu}{\rm GHz}\right)^{-2} \times\left\{\ln\left[4.955\times 10^{-2}\left(\frac{\nu}{\rm GHz}\right)^{-1}\right]+1.5\ln\left(\frac{T_e}{\rm K}\right)\right\} \times\left(\frac{\rm EM}{\rm cm^{-6}pc}\right) \quad (2)$$

[14, 15], where the emission measure, EM, is defined a the integral $\int N_e N_i {\rm d}\ell$. This expression is often approximated as

$$\tau_\nu = 8.235\times 10^{-2}\left(\frac{T_e}{\rm K}\right)^{-1.35} \times\left(\frac{\nu}{\rm GHz}\right)^{-2.1}\left(\frac{\rm EM}{\rm cm^{-6}pc}\right) \quad (3)$$

(see, Altenhoff et al. [16]). The brightness temperature, T_b, from such emission is given by the product

$$T_b = T_e\left(1-{\rm e}^{-\tau_\nu}\right). \quad (4)$$

In the Rayleigh-Jeans region of the spectrum, where $S_\nu = 2k_B T_b/\lambda^2$ in units of W m^{-2} Hz^{-1} sr^{-1}, and assuming emission extended relative to the resolution of the telescope, the resulting flux density from such emission is then given by

$$\left(\frac{S_\nu}{\rm Jy\ bm^{-1}}\right) = 3.07\times 10^4\left(\frac{\nu}{\rm GHz}\right)^2 \times\left(\frac{T_e}{\rm K}\right)\left(1-{\rm e}^{-\tau_\nu}\right)\left(\frac{\Omega_b}{\rm sr}\right), \quad (5)$$

where Ω_b is the beam size in steradians. The integrated flux density of a discrete source, in units of Janskys, may be found by replacing Ω_b in (5) by Ω_s, the source size in steradians.

Where the plasma giving rise to the free-free emission is reasonably uniform in density, this leads to a characteristic radio spectrum which has two components delineated by the frequency at which the optical depth equals unity ($\tau_\nu = 1$), marking the transition from optically thick behaviour to optically thin. In the optically thick regime, the optical depth term in (5) becomes approximately unity and the flux density spectrum rises as ν^2; in the optically thin regime, the optical depth term becomes $\approx\tau_\nu$ and the frequency dependence of τ_ν (see (3)) cancels with the explicit frequency dependence in (5) resulting in a flux density spectrum which varies as $\nu^{-0.1}$. In the optically thin regime the optical depth term tends to unity and the frequency dependence follows the Rayleigh-Jeans spectrum with a ν^2 dependence.

Table 1: Physical parameters for different types of HII regions.

Class	Size (pc)	Density (cm^{-3})	EM (cm^{-6} pc)
Hypercompact	≤0.03	≥10^6	≥10^{10}
Ultracompact	≤0.1	≥10^4	≥10^7
Compact	≤0.5	≥5×10^3	≥10^7
Classical	~10	~100	~10^2

The frequency at which an ionized plasma becomes optically thick/thin depends on its size, density, and to a lesser extent its temperature. The first two of these quantities are combined into the emission measure of such a plasma; the turnover frequency where optical depth equals unity is a strong function of the emission measure.

The emission measure of an ionized plasma surrounding a massive young star can be used to establish the relative age of the object with denser, higher emission measure objects corresponding to younger systems. The highest emission measure objects are referred to as hypercompact HII, or HCHII regions, followed by ultracompact (UCHII), compact (CHII), and classical HII regions in order increase evolution. Typical parameters for such objects are given in Table 1, which is adapted from Kurtz [17]. Often such objects are found grouped together spatially, as the expansion of an HII region into the ambient ISM is thought to cause *triggered* star formation to occur and hence be responsible in part for the creation of additional local compact cores of HII; see Section 3.1.1.

The integrated flux density spectra, following (5), for the four types of HII region summarized in Table 1 are shown in Figure 1(a). The spectra correspond to the nominal parameters as listed in Table 1, a common electron temperature of 10^4 K and scaled to a distance of 10 kpc. The turnover frequencies for the emission measures of compact/ultracompact (1.76 GHz) and hypercompact (47.2 GHz) regions are indicated by vertical dashed lines. Note that the integrated flux density of the compact region is larger than that of the ultracompact due to having an increased size but comparable emission measure. The turnover frequency from the optically thick to optically thin regime as a function of emission measure is shown for a range of electron temperatures in Figure 1(b).

In practice, the optically thick emission of ultra- and hypercompact HII regions tends to have a somewhat shallower observed spectrum than the $S_\nu \propto \nu^2$ behaviour predicted by the uniform density free-free model, with indices in the range $1 \le \alpha \le 2$. This is thought to be due to the fact that such regions are not uniformly smooth, but are instead clumpy along the line of sight [18] with a variety of optical depths present. The morphology of ultra- and hypercompact HII regions is discussed further in Section 3.1.1.

2.1.2. Varying Optical Depth. Frequently the ionized plasma surrounding regions of star formation cannot be well approximated by uniform optical depth but instead has regions of

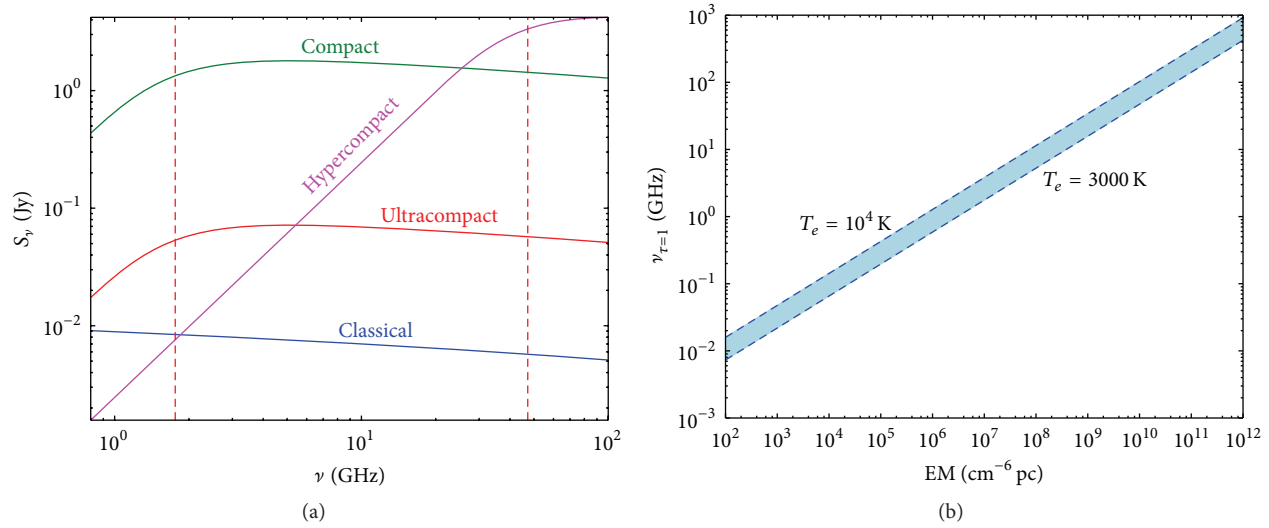

FIGURE 1: (a) Spectra of different types of HII region from Table 1. Red dashed lines indicate turnover frequencies at 1.76 and 47.2 GHz for emission measures of 10^7 and 10^{10} cm^{-6} pc, respectively. (b) Turnover frequency from optically thick to optically thin for free-free emission as a function of emission measure for a range of temperatures.

varying density, resulting in a *partially* opaque plasma. This is particularly the case when considering plasmas in the immediate vicinity of young stellar objects. The spectra from such regions have behaviour that depends not only on the geometry but also on the thermodynamic conditions of the ionized gas. Unlike classical HII regions, where the source of free-free emission is generally due to nearby neutral gas which has been ionized by the strong UV flux from the central star, these plasmas can be associated with stellar winds or ionized jets, both of which are typical in such systems.

The canonical geometry for a stellar wind is that of a spherical region of ionized, isothermal (the polytropic case for the same geometry was considered by Chiuderi and Ciamponi [19], whose derivation preempted the analysis of Reynolds [20] but in a less general form) plasma with a radial density gradient, $n_e(r) = n_0(r/r_0)^{-2}$ [21], where n_0 is the electron density at the inner boundary r_0, which marks the stellar radius. For such an emission region the optical depth through the plasma varies as a function of projected radius on the sky. The unresolved flux density of such a source can be expressed as

$$\left(\frac{S_\nu}{\text{mJy}}\right) = 32.7\left(\frac{n_0}{10^6\ \text{cm}^{-3}}\right)^{4/3}\left(\frac{r_0}{10^{15}\ \text{cm}}\right)^{8/3} \times \left(\frac{\nu}{\text{GHz}}\right)^{0.6}\left(\frac{T_e}{10^4\ \text{K}}\right)^{0.1}\left(\frac{d}{\text{kpc}}\right)^{-2}. \quad (6)$$

The same spectral behaviour is also expected from a conical isothermal jet [22]. Indeed for a more general outflow where the physical conditions are parameterized by different radial dependencies such that $T_e(r) = (r/r_0)^{q_T}$, $\tau(r) = (r/r_0)^{q_\tau}$, and so forth, the spectral index of the radio emission would have the form

$$\alpha = 2 + \frac{2.1}{q_\tau}(1 + \varepsilon + q_T) \quad (7)$$

with $q_\tau = \varepsilon + 2q_x + 2q_n - 1.35q_T$, where τ denotes optical depth, x denotes ionization, n denotes density, T denotes temperature, and ε relates to the opening angle of the jet such that $w = w_0(r/r_0)^\varepsilon$ with w representing the radius of the jet perpendicular to the direction of outflow. For a range of physical situations, this index varies with values $-0.1 \le \alpha \le 1.1$, as listed in Table 1 of Reynolds [22]. For a general outflow, the expression for the integrated radio flux density is

$$\left(\frac{S_\nu}{\text{mJy}}\right) = 4.74F(q_\tau, \alpha)\left(\frac{r_0}{10^{15}\ \text{cm}}\right)^2\left(\frac{\nu}{10\ \text{GHz}}\right)^\alpha \times \left(\frac{\theta_0}{\text{rad}}\right)\left(\frac{\nu_m}{10\ \text{GHz}}\right)^{2-\alpha} \times \left(\frac{d}{\text{kpc}}\right)^{-2}\left(\frac{T_e}{10^4\ \text{K}}\right)\sin i, \quad (8)$$

where $\nu_m = [2\ a_k\ w_0\ n_0^2\ x_0^2\ T_0^{-1.35}(\sin i)^{-1}]^{1/2.1}$ is the turnover frequency from optically thick to optically thin emission, $F(q_\tau, \alpha) = (2.1)^2/q_\tau(\alpha - 2)(\alpha + 0.1)$, and the jet is inclined towards the observer at an angle i. In the specific case of a conical, fully ionized isothermal jet with opening angle $\theta_0 = 2w_0/r_0$ in the plane of the sky, (8) can be rearranged to give an equivalent expression to that of the spherical isothermal wind in (6),

$$\left(\frac{S_\nu}{\text{mJy}}\right) = 1.06\left(\frac{\theta_0}{\text{rad}}\right)^{5/3}\left(\frac{n_0}{10^6\ \text{cm}^{-3}}\right)^{4/3} \times \left(\frac{r_0}{10^{15}\ \text{cm}}\right)^{8/3}\left(\frac{\nu}{\text{GHz}}\right)^{0.6} \times \left(\frac{T_e}{10^4\ \text{K}}\right)^{0.1}\left(\frac{d}{\text{kpc}}\right)^{-2}. \quad (9)$$

Opening angles for outflows from young stellar objects (YSOs) vary with evolution. For example the earliest stage of YSO (Class 0) has highly collimated outflows which become less collimated as they evolve through Class I and, where an outflow remains, leave a wide angle outflow from Class II objects. Typically, however, one may assume that $\theta_0 \leq 0.5$ rad.

Outflows which are collimated ($\varepsilon < 1$) will have shallower spectral indices, typically $\alpha = 0.25$, although pressure confined outflows can exhibit much steeper indices approaching unity. Such steep indices can also be produced by recombining or accelerating outflows where the indices may even exceed unity.

2.1.3. Quantifying Thermal Bremsstrahlung Indirectly. There are two major indirect methods for establishing the expected level of free-free emission from a given region. The first is to use of radio recombination lines (RRLs) to determine the local emission measure and use this to predict the free-free flux density. The integrated line temperature is proportional to both the temperature of the electron plasma and the emission measure,

$$\int T_L \mathrm{d}\nu = 1.92 \times 10^3 \left(\frac{T_e}{\mathrm{K}}\right)^{-1.5} \left(\frac{\mathrm{EM}}{\mathrm{cm^{-6}\,pc}}\right). \quad (10)$$

By assuming an electron temperature, one may determine the emission measure; however generally RRL measurements record both the line temperature and the continuum brightness temperature. By taking the ratio of these two quantities, $\int T_L \mathrm{d}\nu / T_C$, using the expression for brightness temperature in (4), one can find the electron temperature directly,

$$\int T_L \mathrm{d}\nu / T_C = 6.985 \times 10^3 \left(\frac{T_e}{\mathrm{K}}\right)^{-1.15} \left(\frac{\nu}{\mathrm{GHz}}\right)^{1.1}, \quad (11)$$

see, for example, Brown et al. [23] for a review.

The width of RRLs towards HII regions provides a good determinant of the type of region being observed. Typically, diffuse classical HII regions have relatively narrow line profiles with widths of ≈25 km s^{-1} [24], compact HII regions have somewhat broader line width, UCHII region RRLs are broader still with ≈30–40 km s^{-1} [17], and HCHII regions have extremely broad RRLs of 50–100 km s^{-1} and often in excess of 100 km s^{-1} (e.g., NGC 7538; [25]).

The second indirect method for predicting free-free emission is to use Hα emission, which is thought to trace diffuse free-free emission closely as they both arise from the same plasma and therefore their intensities both depend on the same emission measure. The intensity of free-free is given by (5), whereas the intensity of Hα at $\lambda = 6563$ Å (measured in Rayleighs) is given by

$$\left(\frac{I_\alpha}{\mathrm{R}}\right) = 0.36 \left(\frac{\mathrm{EM}}{\mathrm{cm^{-6}\,pc}}\right) \left(\frac{T_e}{10^4\,\mathrm{K}}\right)^{-\gamma} \quad (12)$$

[26], where $\gamma = 0.942 + 0.031 \ln(T_e/10^4\,\mathrm{K})$ [27]. Under the assumption of optically thin free-free emission, combining (3) and (5) and replacing the emission measure term with the rearrangement of (12) leads to the relationship

$$\left(\frac{S_\nu}{\mathrm{Jy\,beam^{-1}}}\right) = 281 \left(\frac{T_e}{10^4\,\mathrm{K}}\right)^{\gamma - 0.35} \times \left(\frac{\nu}{\mathrm{GHz}}\right)^{-0.1} \left(\frac{I_\alpha}{\mathrm{R}}\right) \left(\frac{\Omega_b}{\mathrm{sr}}\right). \quad (13)$$

Although broadly correct, this treatment is somewhat simplistic in its treatment of the emitting species. Whereas free-free emission will arise from *all* ions in the plasma, Hα emission will only arise from $\mathrm{H^+ + e^-}$. Consequently the ratio of free-free to Hα emission will also depend on both the ionization fraction, $x_\mathrm{H} \equiv n(\mathrm{H^+})/n_\mathrm{H}$, and the gas-phase elemental abundance. Without exact knowledge of these conditions the variation in this ratio can be a factor of several (Dong and Draine, 2010).

2.2. Thermal Dust Emission. The spectral behaviour of continuum thermal dust emission is far more coherently expressed than that of free-free emission. Dust spectra are heavily dominated by modified blackbody emission, with an additional subdominant component from the emission lines of individual dust species. The observed continuum flux density from such emission in the Rayleigh-Jeans limit and optically thin limit is characterized as

$$S_\nu \propto \nu^{2+\beta/(1+\Delta)} B_\nu (T_d), \quad (14)$$

where β is the opacity index of the dust population with opacity $\kappa_\nu = \kappa_0 (\nu/\nu_0)^\beta$ (cf. [28]), T_d is the dust temperature, and $B_\nu(T_d)$ is the Planck function.

The opacity index, β, depends on the dust composition and grain size distribution. Smaller grains have larger opacity indices, leading to steeper spectra at longer wavelengths, whereas larger grains such as those found in circumstellar or protoplanetary disks exhibit flatter spectra with low values of β. The opacity index, β, is related to the spectral index of flux density measurements as $\beta = (1 + \Delta)(\alpha - 2)$, where Δ is the ratio of optically thick to optically thin emission. This ratio decreases at longer wavelengths and has been observationally determined in the region 350 μm to 1.3 mm for dark clouds as $\Delta \simeq 0.2$ [29, 30]. Although negative values of β are unphysical, values approaching zero (e.g., [31]) are proposed for the long wavelength tail of the greybody spectrum for young stellar objects, which is dominated by large dust grains in circumstellar/protoplanetary disks. This is substantially lower than that expected for the more diffuse interstellar medium of $\beta_\mathrm{ISM} \approx 1.8$–$2.0$. This difference is due to the change in expected grain size distribution within the dust population, as described previously. For grains with a size distribution $\mathrm{d}n/\mathrm{d}a \propto a^{-p}$, where the grain size $a \leq a_\mathrm{max}$ and $a_\mathrm{max} \geq 3\lambda$, where λ is the wavelength of observation, the measured opacity index will be

$$\beta(\lambda) \approx (p - 3)\, \beta_\mathrm{ISM}. \quad (15)$$

For a typical power-law index of $p = 3.5$ (MRN distribution; [32]), grains with $\beta_\mathrm{ISM} \approx 2$ will have $\beta \approx 1$ when

$a_{\max} > \lambda$ and by extension $\beta \leq 1$ when $a_{\max} > 3\lambda$ [33]. Power-law indices, p, for grain size distributions have been shown to be as low as $p = 3$ for protoplanetary disks (e.g., [34]), which can reduce the expected value of β even further.

Consequently the contribution from thermal dust at microwave frequencies ($\lambda > 3$ mm) is expected to come from the largest grains in the overall population. The additional log normal grain size distribution for very small grains appended to the MRN distribution by Draine and Lazarian [13], as inferred from 12 and 25 μm IRAS data [35], to predict the rotational emission of the small grain population has no effect on the greybody tail of the thermal dust population at these longer wavelengths.

The flux density of dust emission at a single frequency can be used directly to characterize the dust properties of the emitting region. Specifically, the hydrogen column density can be found using

$$\left(\frac{N_{\mathrm{H}}}{\mathrm{cm}^{-2}}\right) = \frac{\Psi}{2.8\, m_{\mathrm{H}}}\left(\frac{S_\nu}{\mathrm{Jy\,beam}^{-1}}\right) \times \left[\left(\frac{\kappa_\nu}{\mathrm{cm}^2\,\mathrm{g}^{-1}}\right)\left(\frac{B_\nu(T_d)}{\mathrm{Jy\,sr}^{-1}}\right)\left(\frac{\Omega}{\mathrm{sr}}\right)\right]^{-1}, \quad (16)$$

where Ψ is the gas-to-dust ratio and m_{H} is the atomic mass of hydrogen. The total (gas + dust) mass can be estimated from the integrated flux density when the distance to the source, d, is known,

$$\left(\frac{M}{\mathrm{M}_\odot}\right) = 4.8\times 10^9 \Psi \left(\frac{S_\nu}{\mathrm{Jy}}\right)\left(\frac{d}{\mathrm{kpc}}\right)^2 \times \left[\left(\frac{\kappa_\nu}{\mathrm{cm}^2\,\mathrm{g}^{-1}}\right)\left(\frac{B_\nu(T_d)}{\mathrm{Jy\,sr}^{-1}}\right)\right]^{-1}, \quad (17)$$

see, for example, Anderson et al. [36]. Both of these quantities also depend on the opacity index β through the dependence of κ_ν on this parameter. Typical normalizations of the opacity function at sub-mm wavelengths are in the range 0.001–0.05 $\mathrm{cm}^2\,\mathrm{g}^{-1}$, and the dust to gas mass ratio, Ψ, is typically assumed to be 100 although there is a large degree of uncertainty in both of these parameters (e.g., [37]). In this paper a dust emissivity of $\kappa_{850} = 0.012\,\mathrm{cm}^2\,\mathrm{g}^{-1}$ (gas + dust), from Ossenkopf and Henning [10] model 5 for icy coagulated grains, and a gas-to-dust mass ratio of 161 (1.5×10^{-26} g of dust per H atom; [38]), assuming gas is 0.89% H by number [39], are assumed.

2.2.1. Free-Free Absorption by Dust. If only free-free emission is involved then the radio spectral index of the flux density with increasing frequency should never be substantially negative. However, this is not the case when free-free is obscured by a dust cloud along the line of sight. The dust and the free-free will have differing optical depths, τ_ν^d and τ_ν^{ff}, respectively, and consequently the recovered flux density will be, following the approach of Rodriguez et al. [40],

$$S_\nu = \frac{2k_B\nu^2}{\mathrm{c}^2}\Omega\left[T_e\left(1-\mathrm{e}^{-\tau_\nu^{\mathrm{ff}}}\right)\mathrm{e}^{-\tau_\nu^d} + T_d\left(1-\mathrm{e}^{-\tau_\nu^d}\right)\right]. \quad (18)$$

Since the optical depth of the dust will be $\tau_\nu^d = N(d)\kappa_0(\nu/\nu_0)^\beta$ where $N(d)$ is the mass column density of the dust and including the Gaunt factor dependence in the free-free optical depth, the resulting absorbed free-free spectral index assumes the complicated form

$$\alpha = 2 + \left\{\beta\tau_\nu^d\mathrm{e}^{-\tau_\nu^d}\left[T_d - T_e\left(1-\mathrm{e}^{-\tau_\nu^{\mathrm{ff}}}\right)\right] - 2\left[1+\left(\ln\frac{T_e^3}{\nu^2}+35.4\right)^{-1}\right]\tau_\nu^{\mathrm{ff}}T_e\mathrm{e}^{-\tau_\nu^{\mathrm{ff}}+\tau_\nu^d}\right\} \times\left[T_e\left(1-\mathrm{e}^{-\tau_\nu^{\mathrm{ff}}}\right)\mathrm{e}^{-\tau_\nu^d} + T_d\left(1-\mathrm{e}^{-\tau_\nu^d}\right)\right]^{-1}. \quad (19)$$

This kind of absorption can produce highly negative spectral indices in principle. However, in practice the dust column densities required are extremely large compared to the expected value in the ambient ISM; see Section 3.1.1.

3. Where Should We Expect to Find Spinning Dust?

Of the seven different environments considered as possible sites for producing spinning dust emission by Draine and Lazarian [13], three are representative of the large scale diffuse interstellar medium or cirrus: the cold neutral medium (CNM), the warm neutral medium (WNM), and the warm ionized medium (WIM); five are directly associated with star formation: dark clouds, molecular clouds, the warm ionized medium, reflection nebulae, and photodissociation regions. The warm ionized medium is a cross-over component as it may be representative not only of large scale diffuse ionized plasmas, but also of hot ionized objects with compact support such as HII regions.

There is some confusion in the literature over terminology in this area, and here I explicitly define my nomenclature. Clouds or dark clouds (DC) are regions of high visual extinction on scales of a few parsecs. They contain large quantities of molecular gas, which often harbours *cores* and active star formation. Cores are defined as compact objects on scales of a few tenths of a parsec and are typically identified at sub-mm wavelengths. Cores can be protostellar or starless, a distinction made on the basis of their SEDs, the presence of an IR source, a molecular outflow, or a compact cm-wave source [41]. Cores identified in the sub-mm are suffixed "SMM," whilst those identified in the infrared are suffixed "IRS." Correspondingly I will refer to dark clouds as being "starless" or "star-forming" based on whether they are known to contain protostellar cores or not. On larger scales of a few parsecs to a few tens of parsecs I will refer to extended regions of presumably interconnected clouds as molecular clouds (MCs), or molecular cloud complexes.

Reflection nebulae (RN) are regions of gas subject to UV flux from nearby stars insufficient to ionize the neutral medium, but strong enough to cause scattering effects which illuminate the dust. Typically they are associated with high mass star formation or particularly luminous premain sequence (PMS; low-mass) stars. In general these low-mass PMS

stars are Herbig Ae/Be stars [42] or FU Orionis objects [43], but in a few cases they may also be illuminated by T Tauri stars (TTS; Class II/III). One such case is the bright reflection nebulae Parsamian 3 [44] associated with a weak-line T Tauri star (WTTS; Class III) binary (possibly triplet; [45]) pair HBC 515 at the apex of the star-forming dark cloud LDN 1622, which will be discussed in more detail later in this review.

Photodissociation regions (PDRs), also sometimes called photon-dominated regions, contain ultraviolet photons from nearby stars, which are not energetic enough to ionize hydrogen and create HII regions, but which can dissociate most molecules. The term remains sufficiently general to include regions that are mostly H_2 or CO but where ultraviolet fluxes still appreciably dissociate other species. In broad terms nearly all phases of the ISM which are not dominated by ionized hydrogen can be considered to be PDRs. The degree of dissociation in PDRs covers a spectrum which includes regions where the penetration of photons leads to a predominantly atomic component with molecular oxygen and hydrogen and atomic carbon, as well as regions where molecular hydrogen and carbon monoxide remain intact and only molecular oxygen is dissociated and which include all gradations of dissociation intermediate to the two. These gradations can also be described by considering the balance between the atomic hydrogen density and the interstellar radiation field (ISRF; e.g., Hollenbach [46]). DL98 defined their PDR scenario as regions with hydrogen density of $n_{\mathrm{H}} = 10^5\ \mathrm{cm}^{-3}$, an ionized hydrogen fraction of 10^{-4} and a more general fraction of ionized species double that of hydrogen. These conditions are typical of PDRs such as those associated with the HII region S140 [47], which represents what might traditionally be termed a PDR, that is a region where neutral hydrogen substantially dominates both ionized and molecular hydrogen, but where other ionized species (such as carbon, oxygen, and silicon) are significant. These other ionized species are identified by their IR emission lines: CII (158 μm), OI (63 μm), and SiII (35 μm). Typically such regions are found predominantly in the outer layers of molecular clouds and in what follows the term PDR will be used in the sense defined by DL98 to denote those regions identified in the literature specifically as these predominantly neutral outer layers where significant line emission from other ionized species has been recorded.

3.1. Targeted Observations. The earliest targeted observations of star formation regions for the purpose of detecting spinning dust emission were made with the Green Bank 43 (140 foot) telescope [48] shortly before it was decommissioned in 1999. These observations targeted a selection of 10 dark clouds, HII regions and infrared sources at 5 and 8–10 GHz, with the intention of constraining an excess at 8–10 GHz relative to any free-free continuum at 5 GHz. Tentative detections were reported towards the dark cloud LDN 1622 and the HII region LPH 201.6+1.6. Later observations revealed that the detection towards LPH 201.6+1.6 was in error [49, 50], but LDN 1622 still remains one of the best candidates for hosting emission from spinning dust grains. These early observations and potential detections lead to a slew of further targeted studies towards a range of objects.

3.1.1. Warm Ionized Medium: HII Regions. The early tentative detection of spinning dust from the HII region LPH 201.6+1.6 [48] had a spectrum which matched the theoretical predictions of DL98 very well, but a magnitude of intensity excess far larger than predicted. This predicted free-free contribution to the flux densities was determined from the Hα survey of Gaustad et al. [51] as described in Section 2.1.3, which indicated an emission measure of EM $\approx 400\ \mathrm{cm}^{-6}$ pc, consistent with a classical HII region (see Table 1).

As described in Section 2.1.1, HII regions are well known as bright radio sources. Although classical HII regions typically have flat radio spectra, with flux density measurements only on the longer wavelength (rising) side of the expected spinning dust spectrum for LPH 201.6+1.6, McCullough and Chen [52] suggested that the excess could in fact be due to the presence of an ultracompact HII region either embedded in or projected against LPH 201.6+1.6 contaminating the data, which would produce such an inverted spectrum at higher frequencies.

Although the emission measure recovered from Hα data did not support the presence of HCHII, see Section 2.1.3, predictions from Hα are strongly affected by optical depth effects and so this alone could not rule out such a theory. However, when combined with low *IRAS* fluxes as pointed out by McCullough and Chen [52], which would suggest an improbably large distance to the potential UCHII region, this possibility seemed remote. In addition, I note that the RRL width towards LPH 201.6+1.6 [24] from observations with a resolution large enough to encompass the IRAS source postulated as the potential contaminant (IRAS 06337+1051; [52]) is only $\Delta V = 22.8 \pm 2.9\ \mathrm{km\,s}^{-1}$. This is low even for diffuse HII regions, which have typical line widths of $\approx 25\ \mathrm{km\,s}^{-1}$ (see Section 2.1.3) as opposed to ultra- and hypercompact HII regions which possess much broader lines widths. Furthermore, the original excess was brought into question by results from the CBI telescope [49], which were subsequently confirmed by the VSA telescope [50], and indeed further observations made with the 100 m Green Bank telescope were unable to reproduce the original rising spectrum seen with the 140-foot telescope (footnote, [49]).

Further studies of HII regions concentrated on larger samples. However, the results were somewhat contradictory. A sample of six HII regions in the Southern hemisphere [53] showed a possible small excess of dust correlated emission relative to *IRAS* 100 μm data with an average emissivity of $3.3 \pm 1.7\ \mu\mathrm{K}\ (\mathrm{MJy\,sr}^{-1})^{-1}$ at 31 GHz over the full sample and a 95% confidence limit of $<6.1\ \mu\mathrm{K}\ (\mathrm{MJy\,sr}^{-1})^{-1}$. The most significant detection was towards RCW 49 which indicated a 3.3σ excess at 31 GHz; see Figure 2. This provided further tentative evidence of some additional mechanism producing emission over the cm-wave band. In contrast a sample of sixteen HII regions in the Northern hemisphere [54] showed no statistically significant excess towards any individual object and on average found a decrease in emission relative to free-free predictions extrapolated from lower frequencies, consistent with the expected steepening of the free-free spectrum at shorter wavelengths [55]. Those objects where a positive

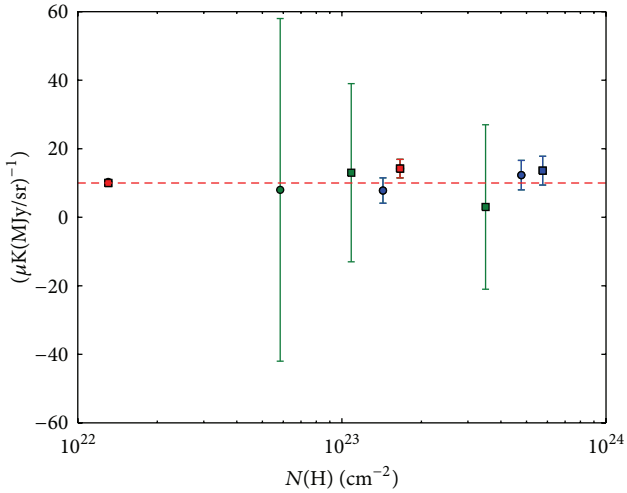

FIGURE 2: Relative emissivity of *excess* microwave emission to 100 μm FIR emission as a function of hydrogen column density, N(H), for HII regions where an excess is detected. Data are shown for excess emission relative to spectra extrapolated using spectral indices fitted to lower frequency data (squares) and using canonical spectral indices for free-free emission (circles) for detections of anomalous microwave emission from Dickinson et al. ([53]; blue points), Scaife et al. ([54]; green points), RCW 175 ([64]; red square), and G159.6–18.5 ([91]; red square). A red dashed line indicates a relative emissivity of 10 μK (MJy/ sr)$^{-1}$ typical of that observed on large scales at high galactic latitudes [80].

excess was observed are shown in Figure 2 where it can be seen that none are statistically distinct from zero.

Aside from the difference in observing frequency, a further potential cause of the discrepancy in AME detection between these two samples of HII regions may be the range of angular scales probed. Anomalous microwave emission was initially detected on large-scales and it should be noted that not only was the sample of Southern HII regions [53] observed with an instrument that had sensitivity to marginally larger angular scales than the Northern sample [54], but also that the Northern sample of HII regions had less associated diffuse emission relative to the resolution of the telescope. Such a differing response to sample composition and spatial sensitivity might indicate that the anomalous microwave emission is present either on larger scales than free-free emission, or may be a consequence of an inverse relationship between VSG abundance and density resulting in a lower spinning dust emissivity as suggested by DL98. The second of these possibilities was proposed by DL98 in the context of dark clouds, which have high densities of molecular gas, rather than HII regions but may also be relevant in this case, although it should be noted that the range of emission measures covered by the two samples was not substantially different.

A significant possibility for misidentification of anomalous microwave emission from HII regions is provided by the presence of ultra- or hypercompact HII regions, such as that suggested by McCullough and Chen [52] for LPH 201.6+1.6, as these may also provide a rising spectral index from lower frequencies. Without additional data at $\nu > 50$ GHz to confirm the peak of the spinning dust SED such contamination is very hard to distinguish.

Unlike low-mass stars, the earliest stages of high-mass star formation where the central object is still undergoing accretion are generally undetectable at radio frequencies. This is because, even though the protostar produces a high enough UV flux to cause significant ionization, the absorption from infalling matter prevents the photons travelling very far from the central source [56]. The radio emission that is seen from ultra- and hypercompact HII regions is thought to occur after accretion finishes and the star evolves onto the main sequence (possibly immediately after or even during the final stages of accretion for hypercompact HII regions) but is still cloaked in the surrounding molecular cloud. During its lifetime on the main sequence, the HII region will evolve from a dense region with the star embedded and expand, revealing the central object, and form a classical nebula. During this expansion the HII region interacts with surrounding or neighbouring molecular clouds by sweeping up material. If the expansion scale is smaller than the size of individual clouds, then this triggers new star formation by effectively "squeezing" the extant dense clumps; if the expansion scale is larger than the size of an individual cloud then a cavity forms surrounded by a rim of collected material which then goes on to form clumps which then collapse triggering new star formation [57]. The first of these mechanisms is considerably faster than the second; however both are observed (e.g., Deharveng et al. [58]; Zavagno et al. [59]; Choudhury et al. [60]. The consequence of this triggered star formation is that different classes of HII region are often found in close proximity. For microwave measurements made with large beam sizes, the contributions of multiple regions of HII of varying emission measure must therefore be accounted for spectrally.

Radio recombination lines (RRLs) provide a useful method for establishing the degree of contamination from denser plasma HII within an unresolved source. Figure 4 shows the distribution of the ratio of microwave excess flux density to 100 μm flux density (following Todorović et al. [61]) with RRL widths, for sources from the VLA Galactic Plane Survey of Todorović et al. [61] and Scaife et al. [54], which have a counterpart in the RRL catalogue of Lockman (see [62]; the HII regions from [53] fall outside the survey area for this catalogue). The average value of RRL width for a classical HII region, see Section 2.1.3, is indicated by a dashed line. Naïvely, one might interpret these data as indicating that UCHII regions are more likely to exhibit a microwave excess; however, if we assume that the dust-to-gas ratio is relatively uniform across these classes, then the ratio of excess microwave emission to 100 μm dust emission should be constant as a function of RRL width. Indeed the dust abundance is expected to be depleted in dense regions (DL98), moreso towards the central star in UC and HCHII regions where temperatures are higher than the dust sublimation temperature. In which case one might expect a negative correlation between RRL width and the excess ratio. It is more likely therefore that the data in Figure 4 indicate that the microwave excess for the two UCHII regions shown is significantly contaminated by an unresolved contribution from dense plasma.

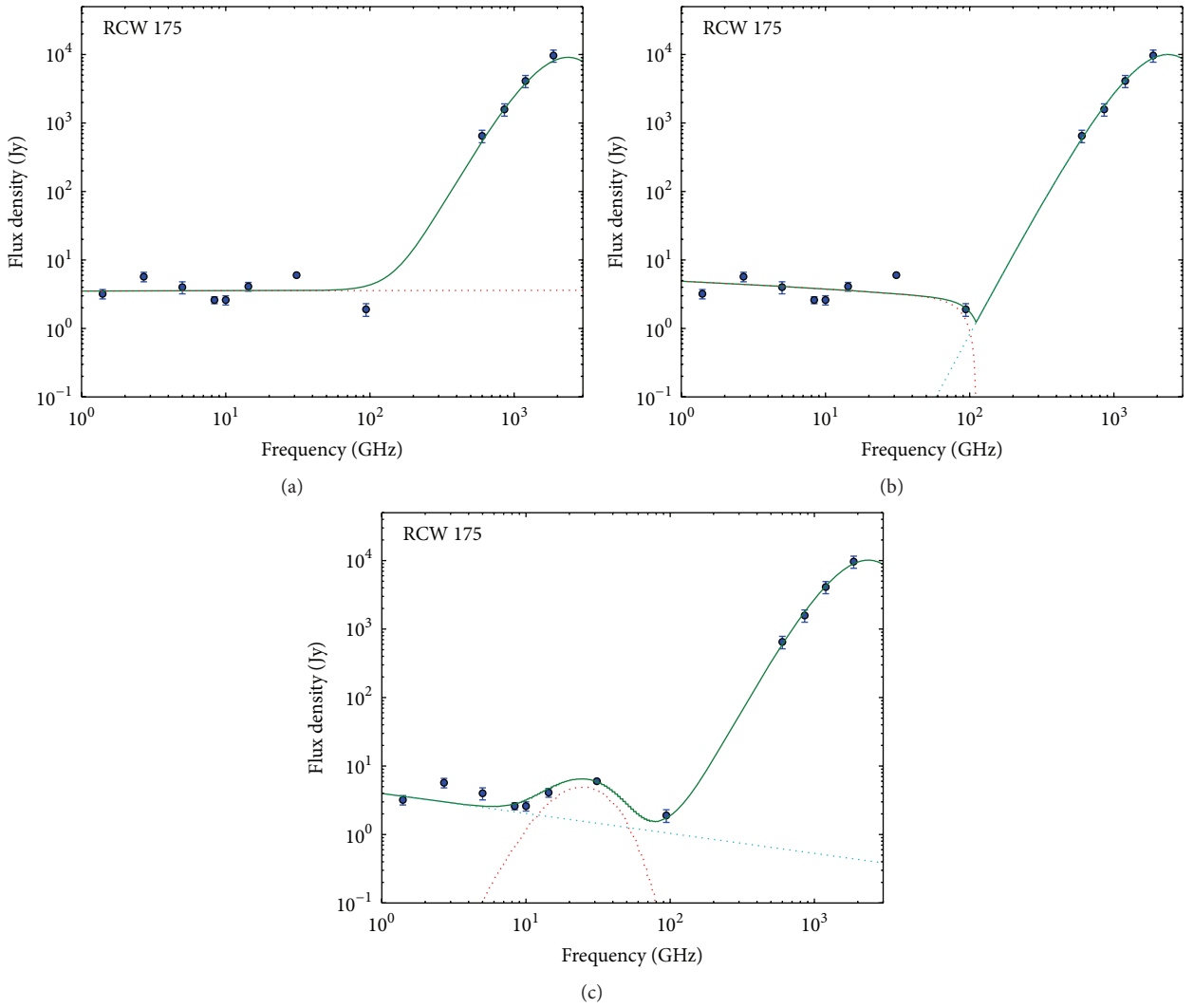

FIGURE 3: SED of RCW 175. (a) Power-law radio emission plus thermal dust greybody. (b) Thermal bremsstrahlung with dust absorption plus thermal dust greybody. (c) Power-law radio emission plus spinning dust (WIM model; DL98) plus thermal dust greybody.

The data point at $\Delta V = 45.1 \pm 3.9\,\mathrm{km\,s^{-1}}$ corresponds to the HII region S211 [63]. Although the measured excess is consistent with zero this object showed the *largest* excess in the sample of 16 Northern HII regions [54], which may also have been due to contamination by an UC/HCHII region.

RCW 175, a more convincing detection of microwave excess from an HII region came from RCW 175 [64], where an excess at 31–33 GHz was reported with an 8.6σ significance. Although RCW 175 is described as an HII region, it is also listed as a *Spitzer* Infrared Dark Cloud (IRDC). Such objects were originally discovered by the *MSX* [65, 66] and *ISO* [67] surveys as dark regions seen against the mid-infrared (MIR) background, in the same way that traditional dark clouds were first identified by Herschel as voids in the optical sky. IRDCs are considered to represent the earliest stages of high-mass star formation in the same way that traditional dark clouds such as those identified by Lynds [68] represent the earliest stages of low-mass star formation, that is, dark clouds will go on to form low-mass stars, whereas the densest IRDCs will go on to form high-mass (massive) stars [69]. IRDCs have low temperatures of <25 K [66, 70] and high densities $n_{\mathrm{H}} > 10^5\,\mathrm{cm^{-3}}$ [66, 71]. Whereas low mass pre- and protostellar cores within dark clouds have masses of a few solar masses, the cores which form in IRDCs can be up to $10^3\,\mathrm{M_\odot}$ (e.g., [72–74]). Current estimates of the ionization degree in IRDCs are similar to those found in PDRs, with upper limits of $\approx 10^{-4}$ [75].

More recently the RCW 175 region was examined in detail by Tibbs et al. [76] who compiled a full SED from radio to infrared wavelengths. The anomalous excess of emission seen at 31 GHz from RCW 175 is largely constrained relative to data at 94 GHz from the *WMAP* satellite. Data at lower radio frequencies have a large amount of systematic scatter, likely due to the extended nature of this object causing difficulties with both flux density estimation and baseline subtraction for single dish telescopes.

In Figure 3 three different scenarios to explain the SED of RCW 175 are examined, based on the physical mechanisms

Table 2: Maximum likelihood parameters from the three models described in Section 3.1.1 fitted to data for RCW 175 [76]. Model fits are shown in Figure 3.

Model	$S_{5\,\mathrm{GHz}}$ (Jy)	α	$N(H)$ (10^{21} cm^{-2})	$S_{100\,\mathrm{GHz}}$ (Jy)	$\Delta \ln Z$
PL+GB	3.54 ± 0.20	0.00 ± 0.03	—	0.75 ± 0.08	—
PL+SD+GB	2.49 ± 0.22	-0.29 ± 0.09	18.6 ± 1.8	0.83 ± 0.08	51.27 ± 0.16
	T_e (K)	EM (cm^{-6} pc)	$N(d)$ (g cm^{-2})	$S_{100\,\mathrm{GHz}}$ (Jy)	
abFF+GB	5800	762 ± 33	0.005 ± 0.002	0.82 ± 0.08	-1.72 ± 0.11

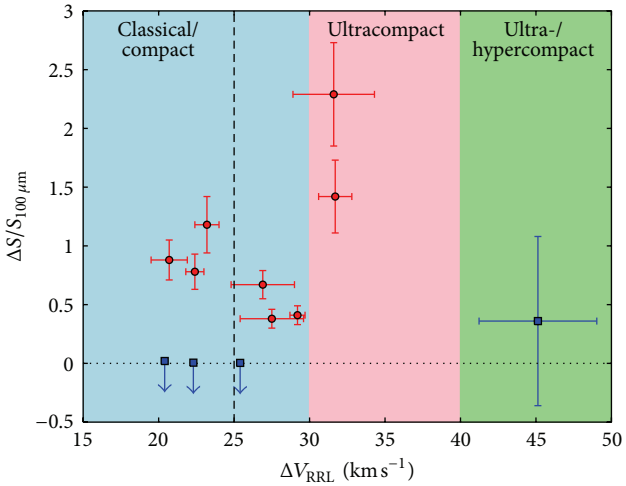

Figure 4: Distribution of excess microwave emission relative to 100 μm emission with RRL width for HII regions. Data are shown from Todorović et al. (see [61]; red points) and Scaife et al. ([54]; blue points). The range of RRL widths corresponding to different types of HII region are indicated, as is the average RRL width for a classical HII region [24].

described in Section 2. Maximum likelihood (ML) parameters for each model were determined using an MCMC based method [77], and the models were ranked using the common dataset [76, Table 4] through calculation of their Bayesian evidence, Z, over a 3σ prior volume around the ML values. The difference in the logarithm of this quantity, $\Delta \ln Z$, with respect to the first scenario is listed in column 6 of Table 2. As the major source of uncertainty in this spectrum arises from the radio data, in each scenario fixed greybody parameters of $\beta = 2.0$ and $T_d = 22.9$ K [76] were assumed, with only the 100 GHz normalization, $S_{100\,\mathrm{GHz}}$, being left as a free parameter.

The first scenario is a simple power-law radio spectrum plus a greybody thermal dust spectrum (PL+GB; Table 2). The radio emission is best fitted by a flat power-law with spectral index $\alpha = -0.00 \pm 0.03$. Although this is close to the canonical value for optically thin free-free emission, see Section 2.1.1, there is significant scatter of the measured data about the fit and notably the data at 31 and 94 GHz are heavily under- and overestimated, respectively.

A model including a thermal bremsstrahlung emission component suffering from dust absorption at high frequencies (scenario 2; abFF+GB), see Section 2.2.1, can account for the dip in flux density at 94 GHz, see Figure 3, relative to lower frequencies. However, in order to produce this degree of absorption, the dust mass column density along the line of sight needs to be high, $N(d) = 0.005 \pm 0.002$ g cm^{-2}. Although such dust mass column densities are not unknown in HII regions they are typically associated with compact cores (e.g., [78]) and not the diffuse medium on large scales. Consequently this degree of absorption is highly unlikely to occur on average towards RCW 175. In addition, these data show no preference for the absorbed free-free model above the simple power-law (PL+GB) model with a Bayes factor of $\Delta \ln Z = -1.72 \pm 0.14$ indicating weak evidence for the preference of the power-law model [79].

A model with both a power-law component and a spinning dust component (scenario 3; FF+SD+GB) is strongly preferred ($\gg 5\sigma$) over both alternative models. The maximum likelihood spectral index, $\alpha = -0.29 \pm 0.09$, is consistent with that found by Tibbs et al. [76]. This is steeper than typically expected from free-free; however the flux densities for this object are found using aperture photometry rather than source fitting due to the extended nature of the emission and, as suggested by Tibbs et al. [76], it is possible that there is some contamination from residual nonthermal background emission which has not been completely excised by the background subtraction.

The emissivity of the excess emission at 31 GHz relative to 100 μm FIR emission for RCW 175 is 14.2 ± 2.7 μK (MJy/ sr)$^{-1}$. Indeed, for all those objects where an excess is detected, the emissivity is reasonably uniform and similar to that observed on large scales at high galactic latitudes of 10 μK (MJy/ sr)$^{-1}$ [80]. The relative emissivity of such objects is plotted as a function of hydrogen column density in Figure 2. The column densities in this figure have been derived from the dust extinction map of Schlegel et al. [81] assuming a conversion factor of $N(\mathrm{H}) = 8 \times 10^{21}$ cm^{-2} for one magnitude $E(B-V)$ [48]. This uniformity would imply that the degree of excess emission is reasonably independent of local column density. However, not all objects exhibit an excess and averaged over larger samples the value of the relative emissivity falls [53, 54, 82]. It is still uncertain why particular objects show an excess and others do not: the nondetections of a microwave excess span the range of column densities shown in Figure 2 and are far more numerous than the known detections.

3.1.2. Molecular Clouds. The Perseus molecular cloud is a well-known star forming cloud nearby in the galaxy. It is associated with three clusters containing premain sequence stars: IC 348, with an estimated age of 2 Myr (and spread of ±1.5 Myr; [83]); NGC 1333, which is less than 1 Myr in

age [84, 85]; and the Per 0B2 association, which contains a B0.5 star [86] and therefore must be less than 13 Myr in age [87]. These clusters therefore all show evidence of star formation activity within the last ~10^7 years. The molecular cloud itself contains a number of previously known protoclusters and isolated protostars and the first full census of its star formation activity was done by Hatchell et al. [88–90] in the sub-mm using a combination of the SCUBA and Harp instruments on the JCMT.

Anomalous emission within Perseus was originally identified using data from the COSMOSOMAS telescope [91] towards the HII region G159.6–18.5 using a combination of COSMOSOMAS data and archival *WMAP* data was well fitted by a combination of WNM and MC spinning dust models from DL98. This detection was confirmed by the VSA telescope [92], which was further able to provide evidence that an excess was seen in multiple separate regions of the cloud. *Planck* data towards Perseus confirmed an excess of microwave emission at 17.1σ [93]. The first measurement of the polarization of anomalous microwave emission was also made towards the Perseus molecular cloud [94], with a detection of 3% fractional polarization. This result was particularly notable as it appeared to rule out the competing mechanism of magnetic dipole fluctuations [13] which would be expected to produce polarized emission approximately an order of magnitude larger.

Additional *Spitzer* analysis of the anomalous regions within Perseus [95] showed that they had no particular enhancement of PAH or VSG population, but that the strength of the ISRF was locally higher. These results indicated that the presence of a VSG population alone was not sufficient to produce the anomalous microwave emission but that the environment of those grains, specifically the ISRF and consequently the equilibrium temperature of the dust, might result in increased emission from spinning dust.

The ρ Ophiuchi molecular cloud [93, 96, 97] lies in the Gould Belt at a distance $d = 135 \pm 15$ pc [98]. It is a region of intermediate-mass star formation and has a high degree of photoionization towards its periphery due to UV flux from its hottest young stars, which heats and dissociates these exposed layers creating photodissociation regions (PDRs), but does not ionise the bulk of the molecular hydrogen in the cloud. The most prominent of these PDRs is ρ Oph W, with n(H) = 10^4–10^5 cm^{-3} [99, 100], which is excited by HD 147889, the earliest star in the ρ Oph star formation complex. The bulk of the mass in the ρ Ophiuchi cloud is situated in the Oph A molecular core [101, 102], a range of values are available for $N(H_2)$ in ρ-Ophiuchus generally (see, e.g., van Dishoeck and Black [103]; Kázmierczak et al. [104]) although the line of sight towards HD 147889 can be used to form rough ideas about the environmental conditions.

An excess of microwave emission was detected towards ρ-Ophiuchus at a significance of 8.4σ by the *Planck* satellite [93]. Both this detection and that of the Perseus molecular cloud were shown to have conical microwave spectra, consistent with the curved peak of the spinning dust SED. The peak itself was found to be flattened in both cases suggesting that several different spinning dust components with different environment conditions were present. This superposition of spectra is perhaps unsurprising given the internal complexity of these molecular clouds and the large angular scales probed by the *Planck* beam, although the extended nature of the microwave emission seen towards both targets relative to this beam once more indicates that AME may be a large-scale phenomenon and is ideally identified using such observations.

3.1.3. Dark Clouds. The dark cloud L1622 has been extensively studied since it provided the first confirmed detection of an anomalous microwave excess in its SED [48]. Although included in a number of catalogues of starless clouds [105, 106] it in fact contains a host of low-mass star formation with at least 32 [107] young stellar objects and premain sequence stars contained in its depths. Notable amongst these is the binary weak-line T Tauri system HBC 515 at the cometary head of the cloud, which is one of the visually brightest known low-mass young stars [108] and is surrounded by the bright reflection nebula Parsamian 3 [44]. The larger cloud is bright-rimmed indicating that the exterior has been ionized by UV flux from a nearby OB type star, probably σ Ori [45], and this is evident both optically and from Hα images of this region (e.g., [51, 109]). The distance to L1622 is uncertain, with estimates favouring distances of either 120–160 pc [109, 110] or 400–500 pc [110–115]. The current weight of favoured distance is the latter, which I will adopt here.

Unlike HII regions, no radio emission is expected from dark clouds as the ionized fraction is thought to be very low. Casassus et al. [116] made the first resolved centimetre-wave image of L1622 using the CBI telescope [117] and confirmed an excess of emission at $\nu > 20$ GHz consistent with the rising radio spectrum first measured by the Green Bank 140 foot telescope [48]. They also demonstrated that the excess emission was more strongly correlated with *IRAS* 12 μm emission than 100 μm emission and suggested that this was evidence for the radio emission arising from the small grain population, which is better traced by the 12 μm emission. A further interesting detail noted for L1622 was that the cm-wave emission was not correlated spatially with the bright ionized rim of L1622, but was rather distributed across the central regions of the cloud. An investigation of the polarization of this emission [118] found a limit of 2.7 (3.5)% at 2 (3) σ, consistent with that expected from spinning dust models and in line with the findings of Battistelli et al. [94] towards the Perseus molecular cloud.

The well-constrained spectrum of the anomalous emission in L1622 was used to investigate the possibility that the excess could be due to rotational emission from fullerenes and fulleranes (hydrogenated fullerenes; [119]). It was found that the excess could be well fitted by a two component model, with the bulk of the species residing in the dark cloud itself and 10 percent in the surrounding cold neutral medium. Much like PAHs, fullerenes are expected to produce strong line emission in the optical and infrared [120] visible with *Spitzer* observations (e.g., [121, 122]).

The first directed sample of a larger number of dark clouds [123] targeted fourteen small diameter clouds selected from previous submillimetre surveys of isolated star forming regions [124]. From identifications in the sub-mm and

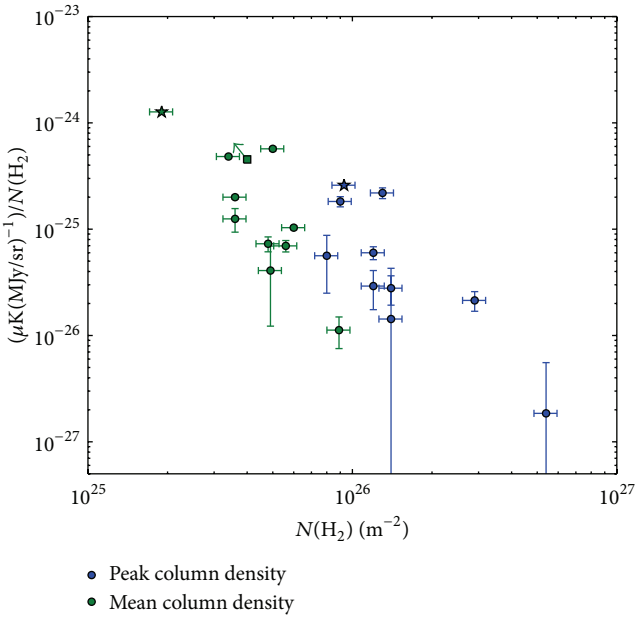

FIGURE 5: Relative emissivity of microwave emission to 100 μm FIR emission as a function of molecular hydrogen column density, $N(H_2)$, for dark clouds. Clouds from Scaife et al. [123, 125] are shown as filled circles, LDN 1622 [116] is shown as filled stars, and LDN 1621 [128] is shown as a filled square.

infrared, only three of these clouds were assumed to be star-forming, with the remainder classified as starless. Of the fourteen selected clouds two were identified as showing clear signs of an anomalous microwave excess, L675 and L1111 (see also [125]), whilst three further clouds were identified as *possible* candidates, L944, L1103, and L1246. These candidates included two of the three clouds known to be protostellar, L944 and L1246.

The relative emissivity of the two clear detections was found to be in excess of that seen on large scales at high galactic latitude with values of 16.4 ± 1.8 and 28.5 ± 3.3 μK $(\mathrm{MJy\,sr^{-1}})^{-1}$ for L675 and L1111, respectively, although there are of course clear environmental differences between diffuse emission at high galactic latitudes and the dense molecular gas of dark clouds. Since these sources were selected from sub-mm data, the column density for each object could be constrained directly from the sub-mm flux density using (16).

The five positive detections from this sample of dark clouds were reobserved at higher resolution at radio frequencies [126, 127] in order to establish whether the microwave emission could be localized more precisely and particularly to investigate whether it followed the same distribution as the cold dust traced by sub-mm observations. A significant finding from these observations was that the dark cloud L675, which was assumed to be starless, hosted a compact radio source coincident with the peak of the 850 μm sub-mm emission. A peak in the sub-mm is not sufficient evidence to demonstrate the presence of star formation as starless cores may also exhibit peaked structure. However, the coincidence of a compact sum-mm peak with a radio point source is strong evidence for protostellar activity [41]. The lack of an infrared point source can be accounted for by the opacity of the dense core, which can often obscure the very earliest stages of protostellar evolution. The presence of a protostar within L675 raised the question of whether it is possible to accurately investigate any correlation of anomalous microwave emission with protostellar activity based on infrared classifications. Investigating this correlation is important not only for providing constraints on physical conditions necessary to produce anomalous microwave emission, but also for assessing the degree of contamination at radio frequencies from protostellar activity. Such contamination is discussed further in Section 4.1.

A further significant result from these high resolution follow-up observations was the first clear morphological correlation of cm-wave radio emission with mid-infrared emission concentrated in *Spitzer* Band 4, indicative of a PAH population [126, 127]. This correlation was detected in the L1246 region, where it had a clear arc-like structure. The remaining objects had no complementary *Spitzer* data available, with the exception of L675, and so the possibility of a similar correlation could not be investigated. However, of the remaining objects only L944 (also star forming) exhibited an unusual morphology in the high resolution observations, with a nebulous radio emission region to the north of the sub-mm core.

For those dark clouds where a microwave excess is detected the degree of emission relative to the FIR 100 μm dust emission appears to be inversely correlated with the column density of molecular hydrogen in the cloud; see Figure 5. The dark cloud sample of Scaife et al. [123] was selected from the sub-mm survey of Visser et al. [124]; and consequently for those objects column densities of molecular hydrogen can be derived directly from the sub-mm flux density (see Table 3 of [124]). Also included in this plot are the dark clouds L1622 and L1621. For L1622 the peak and average column density of molecular hydrogen was derived from the CO measurements of Kun et al. [115] using the relation $N(\mathrm{H_2})/W(\mathrm{CO}) = 1.8 \times 10^{20}\ \mathrm{cm^{-2}/K\,km\,s^{-1}}$. For L1621 [128], the column density of molecular hydrogen was derived from the ^{13}CO measurements of Park et al. [106] assuming a $^{13}\mathrm{CO/H_2}$ ratio of 1.7×10^{-6} [129]. These later molecular line measurements are taken along discrete lines of sight through the cloud and, by comparison to the similar measurements for L1622, will provide values intermediate to the peak and average column densities. Consequently the position of L1621 is shown as a limit on the emissivity relative to the mean column density in Figure 5. It is possible that this negative correlation represents the depletion of small grains in denser environments, as proposed by DL98 when considering the environmental conditions in dark clouds. The microwave excess is correlated in a very similar manner with both the peak and mean column density of molecular hydrogen, which have Pearson correlation coefficients of $r = -0.81$ ($P = 0.004$) and $r = -0.83$ ($P = 0.003$), respectively. The slopes of the correlations are correspondingly consistent with values of -2.08 ± 0.53 and -2.77 ± 0.67.

A similar correlation of 31 GHz intensity with N(H) was demonstrated by Vidal et al. [130], albeit for a less homogeneous sample of clouds, and was also interpreted

as evidence for the microwave emission being associated with the small grain population. The presence of such a correlation is remarkable across so diverse a sample of objects where other environmental conditions such as ionization and temperature vary from source to source, indicating a strong dependence on density.

3.1.4. Reflection Nebulae. Much like dark clouds, reflection nebulae are not expected to emit at radio frequencies as they lack a high degree of ionization. However, significant microwave emission was detected towards the M78 reflection nebula [131], which has been attributed to anomalous microwave emission from spinning dust.

The M78 region is part of the dark cloud L1630 within the Orion molecular cloud. It contains a number of reflection nebulae including NGC 2068, NGC 2071, NGC 2064, and NGC 2067. The nebula NGC 2023, which was used to typify the environmental conditions in reflection nebulae by DL98, is also found in the L1630 dark cloud at a distance of approximately 2.7° from M78. An excess of centimetre-wave emission was detected here using the CBI telescope [131] which was found to be strongly correlated with the infrared emission, although notably here the 12 μm correlation was not stronger than the 100 μm correlation as previously noted by Casassus et al. [116] for L1622, which also hosts a reflection nebula. I note however that the reflection nebulae in these two objects differ somewhat as L1622 is illuminated by low-mass protostars, whereas M78 hosts massive protostars.

3.1.5. Photodissociation Regions. The first, tentative, detection of anomalous microwave emission from a PDR was made with the VSA telescope [50]. This PDR was unusual in nature as it was associated with the supernova remnant (SNR) 3C396 (G39.2–0.3; Green [132]). 3C396 was identified in the *Spitzer* survey of SNRs [133] as having IRAC colours which were not representative of normal interstellar emission; IRAC colours indicated the presence of both shocked ionized gas and two very bright infrared filaments which were identified as PDRs within the SNR, possibly the remnants of old shocks. The excess emission at 33 GHz was significant at the 7σ level, relative to a well-constrained synchrotron spectrum at longer wavelengths.

Strong 31 GHz emission from the ρ-Ophiuchus W PDR was detected with the CBI telescope [134]. Spectrally the emission could not be distinguished from free-free in this case due to a lack of complementary data at lower radio frequencies, and following a detailed study it was concluded that the strong cm-wave emission could have arisen either from spinning dust or from a CII region. Caveats to this were that the CII would have to be optically thick at frequencies $\nu <$ 10 GHz, requiring densities and order of magnitude higher than previously supported by the literature for such a region an and leading to the conclusion that were such emission to be a real possibility the CII regions would have to be distributed in clumps along the line of sight. Such a situation is not unreasonable as it is also invoked to explain the intermediate radio spectral indices seen in HC/UCHII regions; see Section 2.1.1. However, in this case it was suggested that an AME solution was more preferable, a suggestion supported by the later results of the *Planck* satellite towards this region; see Section 3.1.2.

3.2. Other Targeted Observations. In addition to the regions suggested by DL98 as potential sources of spinning dust emission there have been a number of other objects associated with star formation which have been targeted.

3.2.1. Planetary Nebulae. An excess of microwave emission towards 18 planetary nebulae was investigated as possibly arising from spinning dust emission by Casassus et al. [135]. The excess in this case was relative to the higher frequency 250 GHz data from the *SIMBA* telescope. In this case the excess was not found to be consistent with a spinning dust spectrum, but instead proposed as dust extinction, as outlined in Section 2, from a population of needle-like grains. A caveat to this explanation is that it requires extremely low temperatures of $\leq$1 K, which are unphysical. The alternative mechanism of synchrotron emission was also considered, but additional caveats such as the lack of evidence for a CRe population in the vicinity of these objects were also raised. The spectral behavior of these objects at radio frequencies is not typical of spinning dust. The SEDs of the sources tend to be flat at radio wavelengths with a dip at $\nu > 100$ GHz, similar to the absorbed free-free spectral model shown in Figure 3(b).

Additional large surveys of 442 planetary nebulae at 30 GHz from the OCRA-p instrument on the Toruń telescope [136] and 62 planetary nebulae (there is substantial overlap between the samples) at 43 GHz, the 32 m INAF-IRA Noto telescope [137], were also examined for any possible excess emission above a free-free spectrum extrapolated from lower radio frequencies. It was concluded that there was no evidence for an excess of emission which could be considered anomalous.

3.2.2. Extragalactic Spinning Dust. The first detection of anomalous microwave emission from an extragalactic star-formation region was made towards the nearby face-on spiral galaxy NGC 6946 [138, 139]. The detection was made during a series of observations targeting 10 star forming regions within NGC 6946 including the starbursting nucleus, as part of a complementary program to the *Spitzer* Infrared Nearby Galaxies Survey (SINGS; [140]) and the project Key Insights on Nearby Galaxies: a Far-Infrared Survey with *Herschel* (KINGFISH; PI: R. Kennicutt) at 33 GHz with the 100 m Green Bank Telescope. In one of the ten regions (extranuclear region 4), an $\approx 7\sigma$ excess was detected with a spectrum that fitted the high frequency side of the spinning dust peak with a column density of $N_{\rm H} = 3.3 \times 10^{21}\,{\rm cm}^{-2}$, within a factor of two of the column density derived from HI measurements [141]. The low frequency side of the spinning dust spectrum was confirmed to be rising by the AMI telescope [126, 127] where a Bayesian model comparison was used to find that a spinning dust spectrum was preferred by the data above a spectrum which included an UCHII component, although the preference was not at a very high level.

4. Connecting Anomalous Microwave Emission to Protostellar Activity

4.1. Radio Emission from YSOs. Observational studies of dark clouds for identifying anomalous microwave emission have largely concentrated on the arcminute scale emission, neglecting the known small-scale radio emission detected from a significant fraction of protostars [142, 143]. As these investigations become more detailed and explore smaller spatial scales, it is necessary to quantify correctly this emission in order to avoid confusing it with that arising from spinning dust when observing at resolutions where the two may not be easily distinguishable. Historically, a large number of radio protostar searches and surveys (e.g., [143–145]) have been made at 3.6 and 6 cm wavelengths due to the general availability and instrumental efficiency of these frequencies. However, most observations targeted at detecting anomalous microwave emission are made at higher radio frequencies where the spectrum of emission due to spinning dust is thought to peak, ~1-2 cm (DL98). Protostellar observations at such frequencies are available towards a number of discrete sources (e.g., [146–150], hereafter AMB99) as well as through the *Spitzer* follow-up surveys of the AMI telescope at 16 GHz [151–153], which were specifically initiated to investigate the potential relationship between radio emission from YSOs and spinning dust following the identification of a new radio YSO in the AME source L675, which was previously classified as starless [126, 127].

The dense natal dust envelopes which surround YSOs can often conceal their embedded protostars at infrared wavelengths. However, the longer wavelength radiation in the radio band does not suffer to the same extent and is capable of penetrating the dust shell to make such objects detectable at radio frequencies. This radio emission is in addition to that of thermal dust, which is expected to have a spectrum that falls off steeply at long wavelengths, and has been observed to possess a spectrum rising with frequency, indicating that it occurs as a consequence of free-free from partially optically thick ionized plasma, see Section 2.1.2, with spectral indices in the range $0.1 \leq \alpha \leq 2$. In more high-mass stars the physics behind the ionization required to produce radio free-free emission is reasonably well understood as arising from photoionization due to the strong UV flux from such objects. For low-mass objects, multiple mechanisms have been proposed to produce the ionization responsible for free-free emission in the immediate vicinity of YSOs. Similarly to the high-mass case, where a high enough ionizing flux is present (generally in later type T Tauri stars), photoionization may also support an embedded HII region [39]. Otherwise a fully ionized stellar wind, again associated more often with premain sequence stars than YSOs, could be responsible for radio emission [21, 154], as could a partially ionized, collimated outflow [20]; see Section 2.1.2 for expected flux densities. Shock ionization, such as that arising from the accretion shock on the surface of protostellar discs, may heat infalling gas sufficiently to produce radio emission [155, 156]. Alternatively the powerful molecular outflows from young protostars may also cause shock ionization as they encounter the surrounding envelope [154, 157, 158], which will produce a free-free flux density proportional to the outflow force (also called momentum flux), $F_{\rm out}$, which is equivalent to the rate of outflow momentum and is often calculated as $F_{\rm out} = P/\tau_{\rm dyn}$. At a wavelength of 2 cm the expected flux density from such shock ionization can be computed as

$$\left(\frac{S_{\lambda=2\,\mathrm{cm}}}{\mathrm{mJy}}\right) = 3.4\times10^{3}\eta\xi(\tau)^{-1} \times\left(\frac{F_{\rm out}}{\mathrm{M}_{\odot}\ \mathrm{yr}^{-1}\,\mathrm{km\,s}^{-1}}\right)\left(\frac{d}{\mathrm{kpc}}\right)^{-2} \tag{20}$$

(see [126, 127, 159]), where $\eta = (\Omega/4\pi)$ is the fraction of the stellar wind being shocked and the factor $\xi(\tau) = \tau/(1-\mathrm{e}^{-\tau})$ allows for the fact that the radio emission may not be optically thin [160], although this dependence on the optical depth, τ, is very weak.

In the case of low-luminosity protostars, the last of these mechanisms, that of shock ionization associated with the outflow, is often favoured. Although there is considerable uncertainty in measurements of outflow force, most recovered values for observed protostellar jets are considered energetically viable to explain the observed cm-wave radio emission [143]. Shock ionization along the length of these outflows is also supported by very high angular resolution maps of the radio emission [159, 161]; which have revealed radio emission distributed along molecular outflows or extended in a direction consistent with those outflows. In a few cases, however, the increasing sensitivity of the molecular observations required to determine the outflow force has revealed weaker and weaker outflows (e.g., [162, 163]) where the momentum flux appears insufficient to explain the measured radio emission (e.g., [151]). Again this may be explained in specific cases by uncertainties in estimation of momentum flux [164], although it is likely that in others a combination of the above mechanisms is required to account for the observed radio emission.

A strong correlation between radio and bolometric luminosity has been known for some time in the case of YSOs [143], and recent surveys have shown that this correlation appears to hold towards lower luminosities [153]; see Figure 6(a). These recent surveys have also altered the historical bias of radio observations of protostars towards higher luminosities, as can be seen in the grey hatched area of Figure 6(b). This bias was largely a consequence of observational constraints and ongoing improvements in instrumental sensitivity have allowed this distribution increasingly to tend more towards that recovered from blind infrared surveys, although there are still substantial improvements to be made. At low luminosities, potentially large populations of YSOs, as predicted by theoretical models of YSO evolution (e.g., [165]; red hatched area), still remain to be discovered. However, the measured correlation may allow one to predict the contribution of protostars, where identified, to the integrated microwave emission from star forming regions based on their measured bolometric luminosities. The level of this "contamination" when identifying the amount of anomalous microwave emission on large scales is expected to be low given current observational evidence, with typical radio flux densities

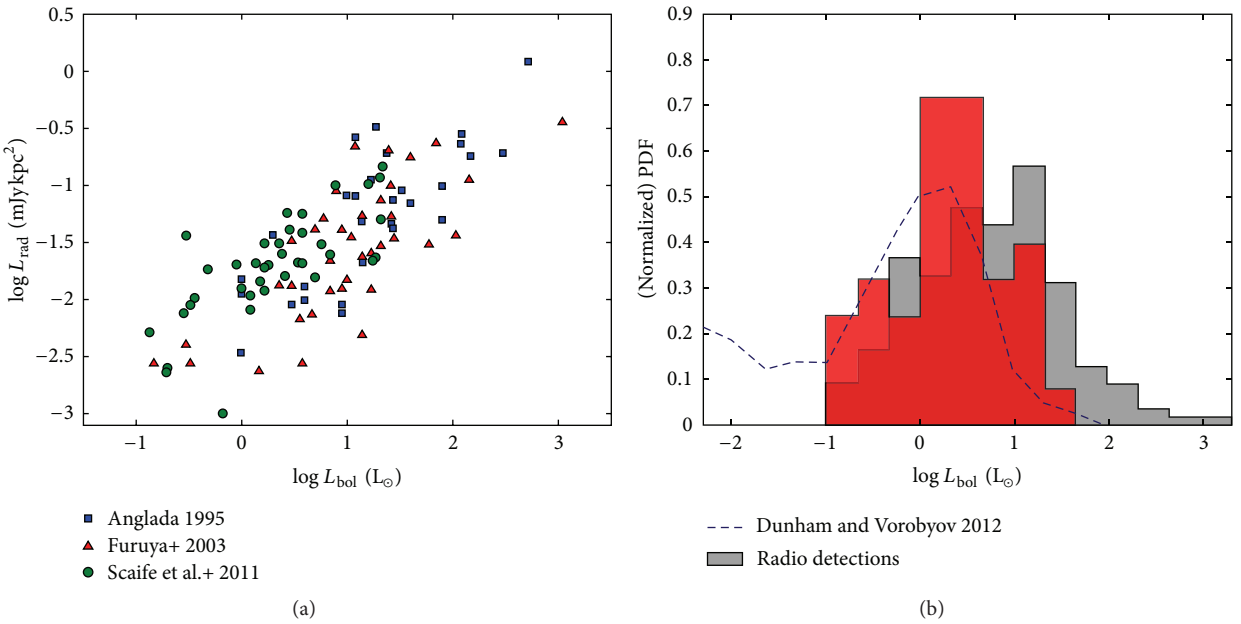

FIGURE 6: (a) Distribution of radio luminosity, L_{rad}, with bolometric luminosity, L_{bol}, for YSOs (figure reproduced from [164]); (b) distribution of radio detected YSOs as a function of bolometric luminosity, compared to the expected distribution of YSOs from Dunham and Vorobyov [165]. Grey hatching indicates objects from the combined catalogues of Anglada [143], Furuya et al. [188], and Scaife et al. [151–153]. Red hatching indicates the objects detected at 16 GHz [151–153].

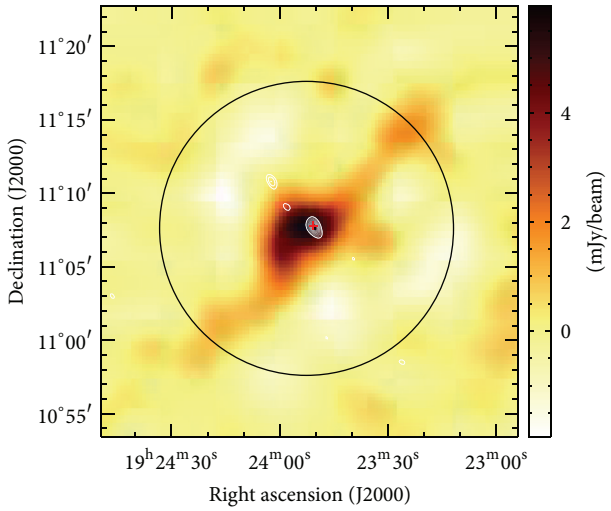

FIGURE 7: L675 star-forming dark cloud. Greyscale shows the anomalous emission on large scales as observed with the AMI telescope [123, 125], and white contours show the compact radio emission from the proposed YSO [126, 127] with contours at intervals of $5\sigma_{rms}$. The position of the sub-mm peak from 850 μm data [124] is marked as a red cross.

for young stellar objects in the range 100–500 μJy. Even considering the possibility of a population of YSOs missed by infrared surveys due to opacity effects, it seems unlikely that such radio emission can account for the anomalous component due to spinning dust as, in addition to the low flux densities expected from such objects, the emission from YSOs is in general highly compact (although there are notable exceptions, e.g., CB188; [151]), whereas the anomalous microwave emission attributed to spinning dust appears on much larger scales; see Figure 7.

A connection between the presence of active star formation within a dark cloud and the identification of a spinning dust component is more difficult to quantify. The observational uncertainties surrounding the identification of heavily embedded, low luminosity YSOs have led to the proposition that many clouds currently considered to be starless, including a number not previously thought to even be undergoing collapse, do in fact host star formation. This possibility creates complications when investigating the correlation of those clouds hosting star formation with those which are associated with anomalous microwave emission, as highlighted by the case of L675 [126, 127] and this remains an important open question. However, the possibility that the excess radio emission associated with spinning dust may be confused by radio emission from YSOs seems remote.

Indeed the inverse correlation of spinning dust emissivity with column density of molecular hydrogen, see Figure 5, suggests that the anomalous emission is in particular *not* associated with the earliest stages of star formation, which tend to occur in more dense environments. This premise also seems to be supported by the distribution of large scale anomalous radio emission in the Perseus molecular cloud. The morphology of this emission avoids the densest regions of star formation traced by sub-mm emission, Figure 8, where the youngest objects are found [89, 90] but are more correlated with the 24 μm emission traced by *Spitzer* MIPS [95].

4.2. PAH Populations in Star Formation Regions and the Interstellar Radiation Field. The connection between anomalous

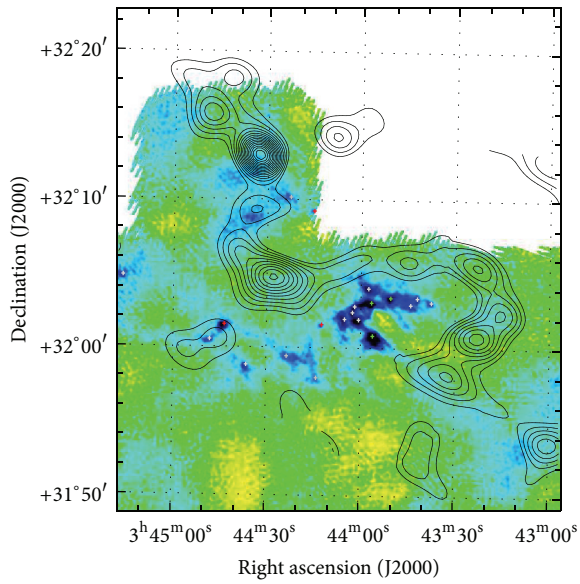

FIGURE 8: Perseus molecular cloud. Contours show radio emission at 16 GHz from the AMI telescope [189] with contours at intervals of 0.25 mJy beam^{-1} ($\sim 5\sigma$) overlaid on greyscale 850 μm data from SCUBA ([89, 90]; J. Hatchell, priv. comm.). The greyscale has been saturated at 500 mJy beam^{-1} (dark blue) to bring out the large-scale features. Crosses indicate the positions of Class 0 (green), Class I (red), and starless cores (grey).

microwave emission and polycyclic aromatic hydrocarbon (PAH) molecules was suggested by DL98, who attributed the emission to such very small grains. These PAH molecules represent the extension at small sizes of the standard grain size distribution (e.g., MRL; see Section 2.2) to molecular dimensions. Such grains are abundant and ubiquitous in the ISM and are generally identified in the mid-infrared (MIR) where stochastic heating from UV photons leads to spectral emission lines at 3.3, 6.2, 7.7, 8.6, and 11.3 μm [166]. Within the dust population it is largely these very small grains/molecules control the overall heating and ionization balance in the ISM and they consequently constitute a very important component in the evolution and chemical balance of star formation regions [167]. Since the strength and prevalence of PAH emission features trace the UV flux, PAH emission has also been proposed as a tracer of star formation [168]. PAH features are particularly bright in the local environment of early type stars such as those associated with HII regions and reflection nebulae (RNe), although they are also detected in the diffuse ISM, planetary nebulae (PNe), and on the surface of protoplanetary disks, as well as in low redshift extragalactic sources such as AGN. The PAH molecules themselves are expected to be produced by fragmentation of larger graphitic grains primarily through the action of interstellar shocks such as those produced by supernovae [169]. However, identifying regions of PAHs associated directly with known supernova remnants (SNRs) is problematic due to projection effects as well as a potential lack of UV illumination necessary for PAH line emission. In a sample of 95 supernova remnants only four were identified in a *Spitzer* survey as having IR colours suggestive of PAH populations [133], including the SNR 3C396 (see Section 3.1.5).

Although PAH emission is seen from such a wide variety of galactic objects, the relative strength of this emission to the FIR continuum varies as a function of source type. This is of course true for the dust continuum also; HII regions show a strong dust continuum from thermal dust emission with relatively weak PAH spectral features, whereas objects such as RNe have much weaker thermal dust continua due to their lower temperature, but stronger PAH line emission. There is a reasonably smooth trend in the emission of such objects from those with a strong thermal continuum and little PAH line emission, such as that seen in compact HII regions, to those with stronger line emission and weaker continuum, such as the diffuse ISM and RNe. This evolution is illustrated in Figure 9(a), which is adapted from the empirical results of Peeters et al. [168]. Certainly this evolution also has a dependence on local conditions and environment, and a key example of this is the Orion Bar (indicated in Figure 9(a)) which is considered an optically visible, that is, more transparent, HII region and is more similar in terms of the ratio of line emission to continuum to RNe than compact HII regions.

The strength of PAH line emission is also related to the interstellar radiation field (ISRF), which is typically normalized to the measurements of Habing (an alternately used normalization is that of Draine [170]) [171] from which the energy density of the ISRF is 1.6×10^{-3} erg cm^{-2} s^{-1}. The normalized ISRF is denoted G_0 (see, e.g., [172]). The ratio of this PAH strength to FIR continuum is an indicator of the abundance ratio of PAH molecules to larger dust grains as it measures the relative number of photons from the ISRF absorbed by the PAH molecules relative to those dust grains. For HII regions the amount of PAH line emission relative to the FIR continuum is reasonably uniform for a broad range of G_0 (approximately three orders of magnitude), see Figure 9(b), before sharply decreasing at $G_0 \simeq 10^6$. Observationally more compact regions of HII have higher values of G_0 due to their higher UV photon flux but their PAH line emission is reduced, possibly due to destruction of the PAH molecules by strong UV flux or alternatively by increased absorption of the UV photons by larger dust grains in the higher density environment. Certainly PAH molecules "compete" more successfully for UV photons in diffuse regions [168] such as RNe, as indicated in Figure 9(b). The Orion Bar is also indicated in this plot as it is a well-known outlier. The microwave emission from very small spinning dust grains, proposed to be PAH molecules, is expected to be largely independent of the ISRF (DL98), while the strength of line emission from PAH molecules is expected to depend approximately linearly on the ISRF [173]. Consequently the ratio of continuum microwave emission to PAH emission line strength, both arising from a population of PAHs, should be inversely proportional to the ISRF [134]. Accordingly direct correlation studies between microwave emission and MIR tracers of PAH emission should have the MIR data corrected for the ISRF, and indeed this has shown to lead to tighter correlation of these data [130].

In spite of the global trends illustrated in Figure 9 the relationship between PAH emission and the ISRF in

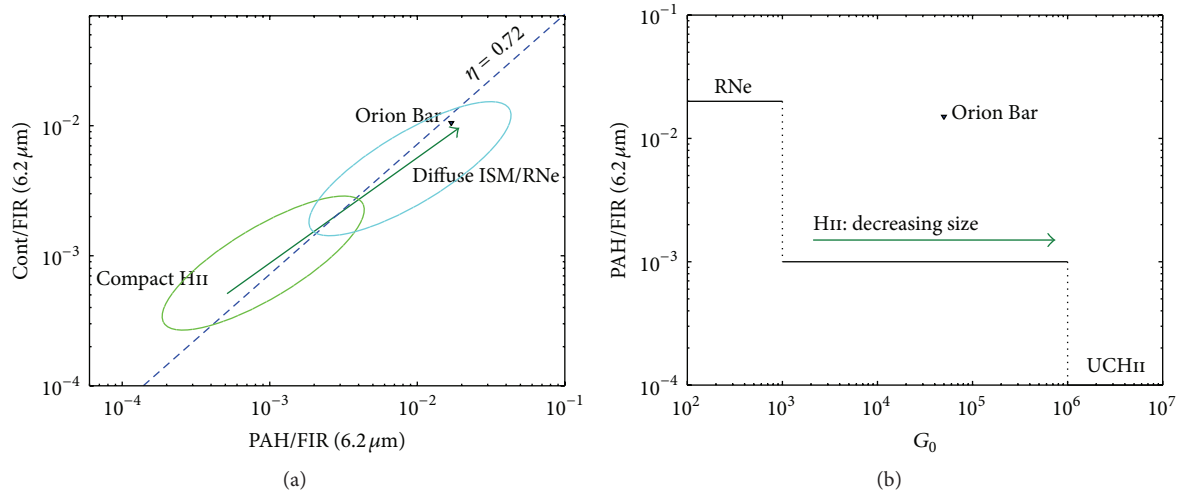

Figure 9: (a) Relationship between the ratio of 6.2 μm emission line feature to the FIR continuum and the ratio of 6.2 μm continuum to FIR continuum for typical galactic objects such as HII regions, RNe, and the diffuse ISM. The dashed line indicates the PAH continuum ratio of 0.72; see text for details. (b) Ratio of 6.2 μm emission line feature to the FIR continuum as a function of the ISRF, G_0, for a range of galactic objects. Figures adapted from Peeters et al. [168].

individual objects is heavily dependent on local conditions and can vary by a significant degree within a source. Furthermore, in contrast to the proposed connection of anomalous microwave emission to PAHs (DL98), the observed correlation of anomalous microwave emission within individual regions has been shown to be a stronger function of ISRF than PAH mass abundance on both large scales in the Perseus molecular cloud [92] and smaller scales within the RCW 175 HII region [76].

5. Observational Issues

There are a number of observational issues which affect the identification of spinning dust emission. These stem from the fact that in order to make a (nonstatistical) detection the SED of the observed object must be well constrained from 1–100 GHz. This presents an immediate problem in terms of available data, with objects that are heavily studied at $\nu \approx 1$ GHz generally not being studied at $\nu \approx 100$ GHz and vice versa. Consequently there is often a gap in available data on either the rising, or the falling, side of the spinning dust SED leaving an uncertainty. This was the case for the Helix planetary nebula which was originally misidentified as having a spinning dust component to its spectrum [174] due to a lack of data at lower radio frequencies concealing the fact that it in fact had a spectrum consistent with free-free emission [123, 125]. Aside from this issue there are also two other circumstances which may contribute significantly to the limitation of identifying an excess of emission at microwave frequencies relative to other mechanisms.

5.1. Calibration Scales. The majority of radio telescopes operating from 1–15 GHz are calibrated from the scale of Baars et al. ([175]; B77), although notable exceptions to this are the Effelsberg 100 m telescope and the Westerbork Synthesis Radio Telescope (WSRT) which employ subtly different flux density scales. Outside this frequency range, the B77 flux scale is known to have a number of issues. At low frequencies it is affected by the secular decrease of Cas A (e.g., [176]), and at higher frequencies it is both incomplete and the resolved structure of Cas A which becomes visible at the higher resolution of many telescopes at shorter wavelengths starts to become an issue. Additionally, for comparison of datasets compiled over long periods of time, the secular decrease of Cas A (and indeed Tau A) must also be accounted for.

Unlike radio telescopes, submillimetre instruments are typically calibrated from planets or bright planetary nebulae. For example the *SCUBA* instrument at the JCMT uses Mars, Uranus, and Neptune as primary calibrators. Long term radio monitoring of Mars has shown that the flux scale of B77 is low relative to the Mars scale at $\nu > 4$ GHz (Rick Perley, priv. comm.). Without correction, this discrepancy can create an artificial excess of emission at frequencies above 4 GHz relative to longer wavelengths. CMB instruments also tend to utilise planets for calibration, notably Jupiter for the ground-based CBI and VSA telescopes [177] as well as for space-based missions such as *WMAP* [178].

More recently the Perley-Butler 2010 flux scale which uses the emission of Mars at frequencies $\nu > 5$ GHz as predicted by the model of Rudy et al. [179] and adjusted to the absolute *WMAP* emission scale [178] has become a broad frequency standard for 1–50 GHz. However, older archival flux densities may often be tied to scales which differ by several percents and are only valid over certain frequency ranges.

5.2. Flux Loss Issues. A further issue with compiling spectra over a range of frequencies is that in the case of extended objects two telescopes operating at the same frequency may measure completely different flux densities depending on the range of angular scales to which they are sensitive. For synthesis telescopes (interferometers), this may involve the loss of flux density not only on angular scales larger than the

shortest separation of their elements, but also on intermediate scales where there is a gap in the *uv*-coverage. This is a particular problem when comparing flux densities from CMB synthesis telescopes which are specifically designed to be sensitive to larger angular scales, with lower radio frequency telescopes designed for examining extragalactic radio sources on small angular scales. This difference can artificially create an excess of emission, which may then be interpreted as anomalous. Particular care must be taken in cases where aperture photometry is used to ensure that appropriate angular scales are measured in all constituent datasets.

6. Where Do We Go from Here?

Currently the bulk of observational data on anomalous microwave emission comes from CMB experiments, which probe large angular scales, and these studies are aimed at detecting the continuum radio emission. Large angular scales are important for identifying regions where anomalous microwave emission is significant as available data indicates that the bulk of the radio signal occurs on these scales. However, information on small angular scales is crucial for probing star formation and circumstellar environments in more detail and understanding the anomalous microwave emission with respect to different ISM conditions requires sufficient resolution to separate distinct environments. Increasingly, galactic surveys undertaken from a non-CMB perspective are expected to contribute to the field of AME science, including those mentioned later in this section, and probe the connections between star formation and spinning dust. Understanding this relationship is important not only in terms of examining the microwave emission itself, but also in terms of probing the VSG and PAH dust populations. VSGs play an important role in the chemical and thermal balance of the ISM; see Section 4.2; in addition to controlling the ionization fraction and temperature of the ISM, the smallest grains account for most of the surface area available for catalysis of molecular formation and the potential information which might be provided by the AME data in this regard is currently largely unexplored.

The existence of VSGs is supported by the physical manifestations of their reprocessing of incident starlight. Such reprocessing by a substantial population of carbonaceous nanoparticles could potentially account for both IR emission features and the strong mid-infrared emission component seen by IRAS. However, the true size distribution of VSGs is poorly known as studies of interstellar extinction are relatively insensitive to its details. The MRN dust size distribution is assumed to significantly underestimate the fraction of ISM carbon content contained in this nanoparticle population and was accordingly modified by DL98 in their spinning dust model to include a significant population of VSGs, assumed to be largely PAH molecules.

Observationally determining the true extent of this VSG/PAH population is nontrivial. The MIR spectral emission features produced by PAHs are only produced when the molecules are subjected to a strong UV flux, which is often absent in the case of heavily embedded pre- and protostellar objects due to local opacity effects. In this respect, spinning dust emission will provide a highly complementary measure of the small grain population to MIR PAH emission in the absence of favorable excitation conditions. At high resolution the anticipated MeerGAL survey at 14 GHz, and additionally the proposed ALMA Band 1 instrument [180] will constrain the spinning dust SED at similar resolution to, for example, *Spitzer* or the forthcoming MIRI instrument on the JWST. With such resolution it may be possible to measure the size distribution of VSGs directly from the data. These constraints will also be important in the context of circumstellar and protoplanetary disks, where the proposed population of VSGs may have important implications for disk evolution. Indeed MIR emission lines from PAH molecules have been detected from the disks around Herbig Ae/Be stars [181], indicating that there is a substantial population of these VSGs present—at least on the surface of the disk where they are irradiated by the central star. However, they have not yet been detected in protoplanetary disks due to a lack of strong UV flux. Since spinning dust emission has been observed to be spatially correlated with PAH emission [123], spinning dust may provide a unique window on the small grain population of these disks. Measurements of the true density and mixing of the PAHs through the disk are not possible using their MIR emission, which is dependent on a strongly ionizing incident UV flux to which only the thin exterior layers of the disk are exposed. In contrast, the rotational emission from these grains that occurs in the microwave regime is dependent on the integrated column density through the disk and may provide useful constraints on whether the VSGs contribute substantially to the disk dust population [182].

In addition to targeted studies with ALMA Band 1, at high angular resolution the new MeerKAT telescope will provide an invaluable resource with its uniquely fast survey speed at 14 GHz. The MeerKAT telescope will have a smaller aperture than the currently available Jansky Very Large Array (JVLA), the consequence of which is that the number of pointings for a 14 GHz survey is comparable to that of an JVLA 5 GHz survey (e.g., CORNISH; [183]). Combining this field-of-view with broadband feeds and the large collecting area resulting from 80 antennas means that MeerKAT has a 14 GHz survey speed over 3 times faster than the JVLA (SKA Memo 40). By working at high frequencies, it gains an additional factor for positive spectral index sources: a MeerKAT 14 GHz survey is over 14 times faster than an JVLA 5 GHz survey would be [184]. The planned MeerGAL survey, the first sensitive arcsecond resolution 12–14 GHz survey of the galactic plane, will be carried out using MeerKAT. The primary aim of this survey is to discover and characterise the population of steep positive spectrum objects in the galaxy and search for variability in their flux densities.

A balance between the high resolution data that will be available from instruments such as MeerKAT, ALMA, and the JVLA and the low resolution data from CMB experiments such as *Planck* will be provided by surveys such as the AMI 16 GHz galactic plane survey (AGPS; [185]). With sensitivity to arcminute scales, the AGPS will provide a highly useful resource for identifying regions of anomalous emission on scales of 2–16 arcmin. At this resolution it will be highly effective at isolating this emission relative to the larger scales

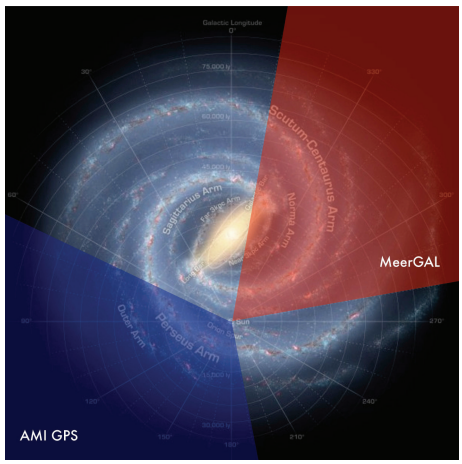

Figure 10: Galactic coverage of the MeerGAL [184] and AMI Galactic Plane Survey [185]. Background image credit: Robert Hurt (SSC Caltech)/NASA/JPL-Caltech.

(≈30 arcmin) measured from all-sky data at 30 GHz with the *Planck* satellite. The AGPS covers the outer galactic plane between $55 \leq \ell \leq 187$ and galactic latitudes of $|b| < 5$; see Figure 10. The AMI telescope has already been successful in providing new identifications of spinning dust and the AGPS offers an excellent opportunity to search new areas of sky aside from pointed observations of known objects.

There is a paucity of surveys currently available in this frequency range due to the comparative expense in terms of observing time of working at higher radio frequencies for fixed aperture telescopes. The cost of a survey with a given sensitivity using a fixed aperture telescope scales as steeply as $\nu^{3.4}$ for objects with negative or slowly falling spectral indices and consequently a 14 GHz survey is 150–2500 times as expensive as a 1.4 GHz survey depending on the spectral index of the objects searched for [184] This has led to a prevalence of low radio frequency surveys, optimal for identifying steep spectrum nonthermal sources. Unfortunately these surveys therefore have a strong selection bias against rising spectrum objects, such as the ultra- and hypercompact HII regions described in Section 2.1.1 and allowing HCHII regions to remain completely undetected in radio surveys at frequencies below 5 GHz until being discovered serendipitously in high frequency observations of UCHII regions. The linear dependence of the turn-over frequency from the optically thick to optically thin thermal bremsstrahlung regime on emission measure, see Section 3.1.1, means that these low frequency surveys preferentially detect objects with low plasma densities and select against dense plasmas. These dense plasmas include not only UC/HCHII regions but also massive stellar winds, ionized jets from low-mass YSOs, and young planetary nebulae [186]. Sources which exhibit anomalous microwave emission due to spinning dust are not dense plasma objects, but due to their rising spectrum from low frequencies they suffer the same bias, which may explain the only relatively recent observational identification of this emission mechanism. It is in part due to this bias that we currently have an incomplete understanding of the physical properties of the objects listed above, not only on an individual basis but also in terms of their underlying populations. From the few major surveys that have been carried out at ~15 GHz, for example, the 9C Ryle Telescope survey [187] and the AT20G survey [138, 139], data are too shallow and/or have sensitivity to a restricted range of (small) angular scales, making it difficult to adequately identify different populations in the highly confused galactic plane.

7. Conclusions

Although observational correlations between the degree of detected anomalous microwave emission and other physical characteristics are emerging for a range of physical conditions, see, for example, Sections 3.1.3 and 4.2, one of the remaining issues is the number of objects that are not detected yet have physical conditions similar to those which are detected. This suggests the existence of a further important physical parameter in the study of spinning dust which has not currently been identified. Doubtless, larger datasets will assist with this characterization but it may be that clues exist in the current data.

Certainly the emerging impression is that those regions of lower density where the ISRF is high provide the most promising environments for detecting anomalous microwave emission. These conditions are linked in the sense that the effective incidence of UV photons on the small grain population is affected by both: a higher ISRF provides a larger incidence rate whereas higher density regions suffer from absorption of UV photons by larger grains. However, a balance is required as the very high ISRF found in some regions may also lead to destruction of the very small grain population.

The prospects for rapid progress in this field are good. Starting from what remains a low level of understanding concerning the necessary triggering mechanisms or local environments suitable for anomalous microwave emission, many questions will be asked and answered with every new dataset that is taken. Whilst information on large scales will be provided by instruments such as the *Planck* satellite, on the smaller scales necessary for probing different environments internal to and in the vicinity of star-formation regions the current and future centimetre-wave surveys with AMI, MeerKAT, and ALMA will undoubtedly contribute extensively to improving our understanding in this area, as will advanced mid-infrared data from instruments such as MIRI on the JWST. In conjunction with further theoretical developments, this combination offers an excellent vehicle for furthering our comprehension of an emission mechanism which is becoming increasingly less anomalous.

References

[1] C. F. McKee and J. P. Ostriker, "A theory of the interstellar medium—three components regulated by supernova explosions in an inhomogeneous substrate," *The Astrophysical Journal*, vol. 218, pp. 148–169, 1977.

[2] S. R. Kulkarni and C. Heiles, "The atomic component," *Astrophysics and Space Science Library*, vol. 134, pp. 87–122, 1987.

[3] R. McCray and T. P. Snow Jr., "The violent interstellar medium," *Annual Review of Astronomy & Astrophysics*, vol. 17, pp. 213–240, 1979.

[4] D. J. Hollenbach and A. G. G. Tielens M, "Photodissociation regions in the interstellar medium of galaxies," *Reviews of Modern Physics*, vol. 71, pp. 173–230, 1999.

[5] R. B. Larson, "Turbulence and star formation in molecular clouds," *Monthly Notices of the Royal Astronomical Society*, vol. 194, pp. 809–826, 1981.

[6] M. M. Mac Low and R. S. Klessen, "Control of star formation by supersonic turbulence," *Reviews of Modern Physics*, vol. 76, pp. 125–194, 2004.

[7] E. M. Leitch, A. C. S. Readhead, T. J. Pearson, and S. T. Myers, "An anomalous component of galactic emission," *Astrophysical Journal Letters*, vol. 486, no. 1, pp. L23–L26, 1997.

[8] B. T. Draine, "Interstellar dust grains," *Annual Review of Astronomy & Astrophysics*, vol. 41, pp. 241–289, 2003.

[9] A. Leger and J. L. Puget, "Identification of the "unidentified" IR emission features of interstellar dust?" *Astronomy & Astrophysics*, vol. 137, no. 1, pp. L5–L8, 1984.

[10] V. Ossenkopf and T. Henning, "Dust opacities for protostellar cores," *Astronomy & Astrophysics*, vol. 291, no. 3, pp. 943–959, 1994.

[11] J. S. Greaves and W. K. M. Rice, "Do all Sun-like stars have planets? Inferences from the disc mass reservoirs of Class 0 protostars," *Monthly Notices of the Royal Astronomical Society*, vol. 412, pp. L88–L92, 2011.

[12] D. Burstein and C. Heiles, "H I, galaxy counts, and reddening—variation in the gas-to-dust ratio, the extinction at high galactic latitudes, and a new method for determining galactic reddening," *The Astrophysical Journal*, vol. 225, pp. 40–55, 1978.

[13] B. T. Draine and A. Lazarian, "Electric dipole radiation from spinning dust grains," *Astrophysical Journal Letters*, vol. 508, no. 1, pp. 157–179, 1998.

[14] L. Oster, "Emission and absorption of thermal radio radiation," *The Astrophysical Journal*, vol. 134, pp. 1010–1013, 1961.

[15] L. Oster, "Free-free emission in the radio-frequency range," *The Astronomical Journal*, vol. 66, p. 50, 1961.

[16] W. Altenhoff, P. G. Mezger, H. Wendker, and G. Westerhout, "Meßprogramme bei der Wellenlänge 11 cm am 25 m-Radioteleskop Stockert," *Veröffentlichungen der Königlichen Sternwärte zu Bonn*, no. 59, p. 48, 1960.

[17] S. Kurtz, "Hypercompact HII regions," in *Proceedings of the International Astronomical Union (IAUS '05)*, Symposium 227, pp. 111–119, 2005.

[18] R. Ignace and E. Churchwell, "Free-free spectral energy distributions of hierarchically clumped H II regions," *The Astrophysical Journal*, vol. 610, no. 1, pp. 351–360, 2004.

[19] C. Chiuderi and G. T. Ciamponi, "Polytropic models of radio stars," *Astronomy & Astrophysics*, vol. 69, pp. 333–339, 1978.

[20] S. P. Reynolds, "Continuum spectra of collimated, ionized stellar winds," *The Astrophysical Journal*, vol. 304, pp. 713–720, 1986.

[21] N. Panagia and M. Felli, "The spectrum of the free-free radiation from extended envelopes," *Astronomy & Astrophysics*, vol. 39, pp. 1–5, 1975.

[22] S. P. Reynolds, "Continuum spectra of collimated, ionized stellar winds," *The Astrophysical Journal*, vol. 304, pp. 713–720, 1986.

[23] R. L. Brown, F. J. Lockman, and G. R. Knapp, "Radio recombination lines," *Annual Review of Astronomy & Astrophysics*, vol. 16, pp. 445–485, 1978.

[24] F. J. Lockman, D. J. Pisano, and G. J. Howard, "Detection of 130 "diffuse" galactic H II regions," *Astrophysical Journal Letters*, vol. 472, no. 1, pp. 173–182, 1996.

[25] R. A. Gaume, W. M. Goss, H. R. Dickel, T. L. Wilson, and K. J. Johnston, "The NGC 7538 IRS 1 region of star formation: observations of the H66a recombination line with a spatial resolution of 300 AU," *Astrophysical Journal Letters*, vol. 438, no. 2, pp. 776–783, 1995.

[26] G. F. Smoot, "Galactic Free-free and H-alpha Emission," http://arxiv.org/abs/astro-ph/9801121.

[27] R. Dong and B. T. Draine, "Hα and free-free emission from the warm ionized medium," *The Astrophysical Journal*, vol. 727, p. 35, 2011.

[28] R. H. Hildebrand, "The determination of cloud masses and dust characteristics from submillimetre thermal emission," *Quarterly Journal of the Royal Astronomical Society*, vol. 24, pp. 267–282, 1983.

[29] J. Rodmann, T. Henning, C. J. Chandler, L. G. Mundy, and D. J. Wilner, "Large dust particles in disks around T Tauri stars," *Astronomy & Astrophysics*, vol. 446, no. 1, pp. 211–221, 2006.

[30] D. Lommen, C. M. Wright, S. T. Maddison et al., "Investigating grain growth in disks around southern T Tauri stars at millimetre wavelengths," *Astronomy & Astrophysics*, vol. 462, pp. 211–220, 2007.

[31] J. B. Pollack, D. Hollenbach, S. Beckwith, D. P. Simonelli, T. Roush, and W. Fong, "Composition and radiative properties of grains in molecular clouds and accretion disks," *Astrophysical Journal Letters*, vol. 421, no. 2, pp. 615–639, 1994.

[32] J. S. Mathis, W. Rumpl, and K. H. Nordsieck, "The size distribution of interstellar grains," *The Astrophysical Journal*, vol. 217, pp. 425–433, 1977.

[33] B. T. Draine, "On the submillimeter opacity of protoplanetary disks," *The Astrophysical Journal*, vol. 636, no. 2, pp. 1114–1120, 2006.

[34] H. Tanaka, Y. Himeno, and S. Ida, "Dust growth and settling in protoplanetary disks and disk spectral energy distributions. I. Laminar disks," *Astrophysical Journal Letters*, vol. 625, no. 1, pp. 414–426, 2005.

[35] F. Boulanger and M. Perault, "Diffuse infrared emission from the galaxy. I—solar neighborhood," *The Astrophysical Journal*, vol. 330, pp. 964–985, 1988.

[36] L. D. Anderson, A. Zavagno, L. Deharveng et al., "The dust properties of bubble H II regions as seen by *Herschel*," *Astronomy & Astrophysics*, vol. 542, article A10, 2012.

[37] T. Preibisch, V. Ossenkopf, H. W. Yorke, and T. Henning, "The influence of ice-coated grains on protostellar spectra," *Astronomy & Astrophysics*, vol. 279, pp. 577–588, 1993.

[38] B. T. Draine and H. M. Lee, " Optical properties of interstellar graphite and silicate grains," *The Astrophysical Journal*, vol. 285, pp. 89–108, 1984.

[39] E. Churchwell, M. G. Wolfire, and D. O. S. Wood, "The infrared emission from dust surrounding newly formed O stars," *Astrophysical Journal Letters*, vol. 354, no. 1, pp. 247–261, 1990.

[40] L. F. Rodriguez, J. Marti, J. Canto, J. M. Moran, and S. Curiel, "Possible radio spectral indices from inhomogeneous free-free sources," *Revista Mexicana De Astronomia Y Astrofisica*, vol. 25, no. 1, pp. 23–229, 1993.

[41] P. Andre, D. Ward-Thompson, and M. Barsony, in *Proceedings of the Protostars and Planets Conference*, p. 59.

[42] G. H. Herbig, "The spectra of Be- and Ae-TYPE stars associated with nebulosity," *The Astrophysical Journal*, vol. 4, p. 337, 1960.

[43] G. H. Herbig, "Eruptive phenomena in early stellar evolution," *The Astrophysical Journal*, vol. 217, pp. 693–715, 1977.

[44] E. S. Parsamian, "Catalogue of cometary nebulae discovered on Palomar maps," *Izv. Akad. Nauk Armyan*, vol. 18, pp. 146–148, 1965.

[45] B. Reipurth, G. Herbig, and C. Aspin, "The multiple pre-main-sequence system HBC 515 in L1622," *The Astronomical Journal*, vol. 139, no. 4, pp. 1668–1680, 2010.

[46] D. J. Hollenbach, in *Astronomical Society of the Pacific Conference Series (ASPC '90)*, vol. 12, p. 167, 1990.

[47] R. Timmermann, F. Bertoldi, C. M. Wright et al., "H_2 infrared line emission from S140: a warm PDR," *Astronomy & Astrophysics*, vol. 315, no. 2, pp. L281–L284, 1996.

[48] D. P. Finkbeiner, D. J. Schlegel, C. Frank, and C. Heiles, "Tentative detection of electric dipole emission from rapidly rotating dust grains," *Astrophysical Journal Letters*, vol. 566, no. 2, pp. 898–904, 2002.

[49] C. Dickinson, S. Casassus, J. L. Pineda, T. J. Pearson, A. C. S. Readhead, and R. D. Davies, "An upper limit on anomalous dust emission at 31 GHz in the diffuse cloud [LPH96] 201.663+1.643," *The Astrophysical Journal*, vol. 643, no. 2, pp. L111–L114, 2006.

[50] A. Scaife, D. A. Green, R. A. Battye et al., "Constraints on spinning dust towards Galactic targets with the Very Small Array: a tentative detection of excess microwave emission towards $_3C_{39}6$," *Monthly Notices of the Royal Astronomical Society*, vol. 377, pp. L69–L73, 2007.

[51] J. E. Gaustad, P. R. McCullough, W. Rosing, and D. Van Buren, "A robotic wide-angle Hα survey of the southern sky," *Publications of the Astronomical Society of the Pacific*, vol. 113, no. 789, pp. 1326–1348, 2001.

[52] P. R. McCullough and R. R. Chen, "An alternative to spinning dust for the microwave emission of LPH 201.663+1.643: an Ultracompact H II Region," *The Astrophysical Journal Letters*, vol. 566, no. 1, article L45, 2002.

[53] C. Dickinson, R. D. Davies, L. Bronfman et al., "CBI limits on 31 GHz excess emission in southern H ii regions," *Monthly Notices of the Royal Astronomical Society*, vol. 379, no. 1, pp. 297–307, 2007.

[54] A. M. M. Scaife, N. Hurley-Walker, M. L. Davies et al., "AMI limits on 15-GHz excess emission in northern H ii regions," *Monthly Notices of the Royal Astronomical Society*, vol. 385, pp. 809–822, 2008.

[55] C. Dickinson, R. D. Davies, and R. J. Davis, "Towards a free-free template for CMB foregrounds," *Monthly Notices of the Royal Astronomical Society*, vol. 341, pp. 369–384, 2003.

[56] E. Churchwell, "Ultra-compact H II regions and massive star formation," *Annual Review of Astronomy and Astrophysics*, vol. 40, pp. 27–62, 2002.

[57] B. G. Elmegreen, "Triggered star formation," *EAS Publications Series*, vol. 51, pp. 45–58, 2011.

[58] L. Deharveng, F. Schuller, L. D. Anderson et al., "A gallery of bubbles. The nature of the bubbles observed by *Spitzer*and what ATLASGAL tells us about the surrounding neutral material," *Astronomy & Astrophysics*, vol. 523, article A6, 2010.

[59] A. Zavagno, L. Deharveng, F. Comerón et al., "Triggered massive-star formation on the borders of Galactic H II regions II. Evidence for the collect and collapse process around RCW 79," *Astronomy & Astrophysics*, vol. 446, no. 1, pp. 171–184, 2006.

[60] R. Choudhury, B. Mookerjea, and H. C. Bhatt, "Triggered star formation and young stellar population in bright-rimmed cloud SFO 38," *Astrophysical Journal Letters*, vol. 717, no. 2, pp. 1067–1083, 2010.

[61] M. Todorović, R. D. Davies, C. Dickinson et al., "A 33-GHz very small array survey of the Galactic plane from $\ell = 27^\circ$ to 46°," *Monthly Notices of the Royal Astronomical Society*, vol. 406, pp. 1629–1643, 2010.

[62] F. J. Lockman, "A survey of radio H II regions in the northern sky," *The Astrophysical Journal Supplement Series*, vol. 71, pp. 469–479, 1989.

[63] S. Sharpless, "A catalogue of H II regions," *The Astrophysical Journal Supplement Series*, vol. 4, p. 257, 1959.

[64] C. Dickinson et al., "Anomalous microwave emission from the H II region RCW175," *The Astrophysical Journal*, vol. 690, no. 2, article 1585, 2009.

[65] S. J. Carey, F. O. Clark, M. P. Egan, S. D. Price, R. F. Snipman, and T. A. Kuchar, "The physical properties of the Midcourse Space Experiment galactic infrared-dark clouds," *Astrophysical Journal Letters*, vol. 508, no. 2, pp. 721–728, 1998.

[66] M. P. Egan, R. F. Shipman, S. D. Price, S. J. Carey, F. O. Clark, and M. Cohen, "A population of cold cores in the galactic plane," *Astrophysical Journal Letters*, vol. 494, no. 2, pp. L199–L202, 1998.

[67] M. Perault et al., "First ISOCAM images of the Milky Way," *Astronomy & Astrophysics*, vol. 315, p. L165, 1996.

[68] B. T. Lynds, "Catalogue of dark nebulae," *The Astrophysical Journal*, vol. 7, p. 1, 1962.

[69] J. Kauffmann and T. Pillai, "How many infrared dark clouds can form massive stars and clusters?" *The Astrophysical Journal Letters*, vol. 723, no. 1, article L7, 2010.

[70] D. Teyssier, P. Hennebelle, and M. Perault, "Radio-millimetre investigation of galactic infrared dark clouds," *Astronomy & Astrophysics*, vol. 382, pp. 624–638, 2002.

[71] S. J. Carey, P. A. Feldman, R. O. Redman, M. P. Egan, J. M. MacLeod, and S. D. Price, "Submillimeter observations of Midcourse Space Experiment galactic infrared-dark clouds," *The Astrophysical Journal*, vol. 543, no. 2, pp. L157–L161, 2000.

[72] J. M. Rathborne, J. M. Jackson, R. Simon, and Q. Zhang, "Infrared dark clouds as precursors to star clusters," *Astrophysics and Space Science*, vol. 324, pp. 155–162, 2009.

[73] N. Peretto and G. A. Fuller, "A statistical study of the mass and density structure of infrared dark clouds," *Astrophysical Journal Letters*, vol. 723, no. 1, pp. 555–562, 2010.

[74] L. A. Wilcock, J. M. Kirk, D. Stamatellos et al., "The initial conditions of high-mass star formation: radiative transfer models of IRDCs seen in the *Herschel* Hi-GAL survey," *Astronomy & Astrophysics*, vol. 526, article A159, 2011.

[75] O. Miettinen, M. Hennemann, and H. Linz, "Deuterium fractionation and the degree of ionisation in massive clumps within infrared dark clouds," *Astronomy & Astrophysics*, vol. 534, article A134, 2011.

[76] C. T. Tibbs, R. Paladini, M. Compiegne, M. C et al., "A multi-wavelength investigation of RCW175: an HII region harboring spinning dust emission," *The Astrophysical Journal*, vol. 754, no. 2, article 94, 2012.

[77] M. P. Hobson and J. E. Baldwin, "Markov-chain Monte Carlo approach to the design of multilayer thin-film optical coatings," *Applied Optics*, vol. 43, pp. 2651–2660, 2004.

[78] K. Arvidsson and C. R. Kerton, "Submillimeter and molecular views of three galactic ring-like H II regions," *The Astronomical Journal*, vol. 141, no. 5, article 153, 2011.

[79] C. Gordon and R. Trotta, "Bayesian calibrated significance levels applied to the spectral tilt and hemispherical asymmetry," *Monthly Notices of the Royal Astronomical Society*, vol. 382, pp. 1859–1863, 2007.

[80] R. D. Davies, C. Dickinson, A. J. Banday, T. R. Jaffe, K. M. Górski, and R. J. Davis, "A determination of the spectra of Galactic components observed by the *Wilkinson Microwave Anisotropy Probe*," *Monthly Notices of the Royal Astronomical Society*, vol. 370, pp. 1125–1139, 2006.

[81] D. J. Schlegel, D. P. Finkbeiner, and M. Davis, "Maps of dust infrared emission for use in estimation of reddening and cosmic microwave background radiation foregrounds," *Astrophysical Journal Letters*, vol. 500, no. 2, pp. 525–553, 1998.

[82] C. Dickinson, "Anomalous Emission from HII regions," http://arxiv.org/abs/0808.0473.

[83] K. L. Luhman, J. R. Stauffer, A. A. Muench et al., "A census of the young cluster IC 348," *Astrophysical Journal Letters*, vol. 593, no. 2, pp. 1093–1115, 2003.

[84] C. J. Lada, J. Alves, and E. A. Lada, "Near-infrared imaging of embedded clusters: NGC 1333," *The Astronomical Journal*, vol. 111, no. 5, pp. 1964–1976, 1996.

[85] B. A. Wilking, M. R. Meyer, T. P. Greene, A. Mikhail, and G. Carlson, "Low-mass stars and substellar objects in the NGC 1333 molecular cloud," *The Astronomical Journal*, vol. 127, no. 2, pp. 1131–1146, 2004.

[86] K. C. Steenbrugge, J. H. J. De Bruijne, R. Hoogerwerf, and P. T. De Zeeuw, "Radial velocities of early-type stars in the Perseus OB2 association," *Astronomy & Astrophysics*, vol. 402, no. 2, pp. 587–605, 2003.

[87] G. Meynet and A. Maeder, "Stellar evolution with rotation V. Changes in all the outputs of massive star models," *Astronomy & Astrophysics*, vol. 361, no. 1, pp. 101–120, 2000.

[88] J. Hatchell, J. S. Richer, G. A. Fuller, C. J. Qualtrough, E. F. Ladd, and C. J. Chandler, "Star formation in Perseus: clusters, filaments and the conditions for star formation," *Astronomy & Astrophysics*, vol. 440, no. 1, pp. 151–161, 2005.

[89] J. Hatchell, G. A. Fuller, and J. S. Richer, "Star formation in Perseus III. Outflows," *Astronomy & Astrophysics*, vol. 472, no. 1, pp. 187–198, 2007.

[90] J. Hatchell, G. A. Fuller, J. S. Richer, T. J. Harries, and E. F. Ladd, "Star formation in Perseus II. SEDs, classification, and lifetimes," *Astronomy & Astrophysics*, vol. 468, no. 3, pp. 1009–1024, 2007.

[91] R. A. Watson, R. Rebolo, J. A. Rubiño-Martín et al., "Detection of anomalous microwave emission in the perseus molecular cloud with the COSMOSOMAS experiment," *The Astrophysical Journal Letters*, vol. 624, no. 2, article L89, 2005.

[92] C. T. Tibbs, R. A. Watson, C. Dickinson and et al., "Very Small Array observations of the anomalous microwave emission in the Perseus region," *Monthly Notices of the Royal Astronomical Society*, vol. 402, pp. 1969–1979, 2010.

[93] P. J. Encrenaz, "A new source of intense molecular emission in the rho ophiuchi complex," *The Astrophysical Journal*, vol. 189, p. L135, 1974.

[94] E. S. Battistelli, R. Rebolo, J. A. Rubiño-Martín et al., "Polarization observations of the anomalous microwave emission in the perseus molecular complex with the COSMOSOMAS experiment," *The Astrophysical Journal Letters*, vol. 645, no. 2, article L141, 2006.

[95] C. T. Tibbs, N. Flagey, R. Paladini et al., "*Spitzer* characterization of dust in an anomalous emission region: the Perseus cloud," *Monthly Notices of the Royal Astronomical Society*, vol. 418, pp. 1889–1900, 2011.

[96] C. A. Kulesa, A. L. Hungerford, C. K. Walker, X. Zhang, and A. P. Lane, "Large-scale CO and [C I] emission in the ρ ophiuchi molecular cloud," *The Astrophysical Journal*, vol. 625, no. 1, pp. 194–209, 2005.

[97] K. E. Young, M. L. Enoch, N. J. Evans II et al., "Bolocam survey for 1.1 mm dust continuum emission in the c2d legacy clouds. II. Ophiuchus," *The Astrophysical Journal*, vol. 644, no. 1, article 326, 2006.

[98] M. A. C. Perryman, L. Lindegren, J. Kovalevsky, E. Hoeg et al., "The HIPPARCOS Catalogue," *Astronomy & Astrophysics*, vol. 323, pp. L49–L52, 1997.

[99] R. Liseau, G. J. White, B. Larsson et al., "Looking at the bright side of the ρ Ophiuchi dark cloud. Far infrared spectrophotometric observations of the ρ Oph cloud with the ISO-LWS," *Astronomy & Astrophysics*, vol. 344, pp. 342–354, 1999.

[100] E. Habart, F. Boulanger, L. Verstraete, G. Pineau des Forêts, E. Falgarone, and A. Abergel, "H_2 infrared line emission across the bright side of the ρ ophiuchi main cloud," *Astronomy & Astrophysics*, vol. 397, no. 2, pp. 623–634, 2003.

[101] A. Wootten, R. Snell, and A. E. Glassgold, "The determination of electron abundances in interstellar clouds," *The Astrophysical Journal*, vol. 234, pp. 876–880, 1979.

[102] A. Wootten, N. J. Evans, N. J. II, R. Snell, and P. vanden Bout, "Molecular abundance variations in interstellar clouds," *The Astrophysical Journal*, vol. 225, pp. L143–L148, 1978.

[103] E. F. van Dishoeck and J. H. Black, "Interstellar C2, CH, and CN in translucent molecular clouds," *The Astrophysical Journal*, vol. 340, pp. 273–297, 1989.

[104] M. Kámierczak, M. R. Schmidt, A. Bondar, and J. KreLowski, "Abundances and rotational temperatures of the C_2 interstellar molecule towards six reddened early-type stars," *Monthly Notices of the Royal Astronomical Society*, vol. 402, pp. 2548–2558, 2010.

[105] C. W. Lee, P. C. Myers, and M. Tafalla, "A survey for infall motions toward starless cores. II. CS (2-1) and N_2H^+ (1-0) mapping observations," *The Astrophysical Journal*, vol. 136, no. 2, p. 703, 2001.

[106] Y. S. Park, C. W. Lee, and P. C. Myers, "A CO Survey toward Starless Cores," *The Astrophysical Journal* , vol. 152, no. 1, article 81, 2004.

[107] B. Reipurth, S. T. Megeath, J. Bally, and J. Walawender, "The L1617 and L1622 cometary clouds in orion," in *Handbook of Star Forming Regions, Volume I*, p. 782, 2008.

[108] G. H. Herbig and K. R. Bell, cels.book, 1988.

[109] B. A. Wilson, T. M. Dame, M. R. W. Masheder, and P. Thaddeus, "A uniform CO survey of the molecular clouds in Orion and Monoceros," *Astronomy & Astrophysics*, vol. 430, no. 2, pp. 523–539, 2005.

[110] J. Knude, C. Fabricius, E. Høg, and V. Makarov, "Distances of absorbing features in the LDN 1622 direction: an application of Tycho-2 photometry and Michigan Classification," *Astronomy & Astrophysics*, vol. 392, no. 3, pp. 1069–1079, 2002.

[111] R. F. Garrison, "The σ orionis clustering," *Publications of the Astronomical Society of the Pacific*, vol. 79, no. 470, p. 433, 1967.

[112] R. J. Maddalena, M. Morris, J. Moscowitz, and P. Thaddeus, "The large system of molecular clouds in Orion and Monoceros," *The Astrophysical Journal*, vol. 303, pp. 375–391, 1986.

[113] W. H. Sherry, F. M. Walter, S. J. Wolk, and N. R. Adams, "Main-sequence fitting distance to the σ Ori cluster," *The Astronomical Journal*, vol. 135, no. 4, pp. 1616–1623, 2008.

[114] J. Bally, J. Walawender, B. Reipurth, and S. T. Megeath, "Outflows and young stars in orion's large cometary clouds L1622and L1634," *The Astronomical Journal*, vol. 137, no. 4, p. 3843, 2009.

[115] M. Kun, Z. Balog, N. Mizuno et al., "Lynds 1622: a nearby star-forming cloud projected on Orion B?" *Monthly Notices of the Royal Astronomical Society*, vol. 391, pp. 84–94, 2008.

[116] S. Casassus, G. F. Cabrera, F. Forster, T. J. Pearson, A. C. S. Readhead, and C. Dickinson, "Morphological analysis of the centimeter-wave continuum in the dark cloud LDN 1622," *The Astrophysical Journal*, vol. 639, no. 2, article 951, 2006.

[117] S. Padin, M. C. Shepherd, J. K. Cartwright et al., "The cosmic background imager," *Publications of the Astronomical Society of the Pacific*, vol. 114, pp. 83–97, 2002.

[118] B. S. Mason, T. Robishaw, C. Heiles, D. Finkbeiner, and C. Dickinson, "A limit on the polarized anomalous microwave emission of lynds 1622," *Astrophysical Journal Letters*, vol. 697, no. 2, pp. 1187–1193, 2009.

[119] S. Iglesias-Groth, "Hydrogenated fulleranes and the anomalous microwave emission of the dark cloud LDN 1622," *Monthly Notices of the Royal Astronomical Society*, vol. 368, pp. 1925–1930, 2006.

[120] C. C. Henderson and P. A. Cahill, "$C_{60}H_2$: synthesis of the simplest C_{60} hydrocarbon derivative," *Science*, vol. 259, no. 5103, pp. 1885–1887, 1993.

[121] J. Cami, J. Bernard-Salas, E. Peeters, and S. E. Malek, "Fullerenes in circumstellar and interstellar environments," in *Proceedings of the International Astronomical Union (IAUS '11)*, vol. 7 of *Symposium S280*, pp. 216–227, 2011.

[122] A. Garcia-Hernandez, "On the formation of fullerenes in H-rich circumstellar environments," in *Proceedings of the International Astronomical Union (IAUS '11)*, Symposium 280, 2011.

[123] A. M. M. Scaife, N. Hurley-Walker, D. A. Green et al., "An excess of emission in the dark cloud LDN1111 with the Arcminute Microkelvin Imager," *Monthly Notices of the Royal Astronomical Society*, vol. 394, pp. L46–L50, 2009.

[124] A. E. Visser, J. S. Richer, and C. J. Chandler, "A SCUBA survey of compact dark Lynds clouds," *Monthly Notices of the Royal Astronomical Society*, vol. 323, no. 2, pp. 257–269, 2001.

[125] A. M. M. Scaife, N. Hurley-Walker, D. A. Green et al., "AMI observations of Lynds dark nebulae: further evidence for anomalous cm-wave emission," *Monthly Notices of the Royal Astronomical Society*, vol. 400, pp. 1394–1412, 2009.

[126] A. M. M. Scaife, M. Scaife, B. Nikolic et al., "Microwave observations of spinning dust emission in NGC6946," *Monthly Notices of the Royal Astronomical Society*, vol. 406, pp. L45–L49, 2010.

[127] A. M. M. Scaife, D. A. Green, G. G. Pooley et al., "High-resolution AMI Large Array imaging of spinning dust sources: spatially correlated 8 μm emission and evidence of a stellar wind in L675," *Monthly Notices of the Royal Astronomical Society*, vol. 403, pp. L46–L50, 2010.

[128] C. Dickinson, S. Casassus, R. D. Davies et al., "Infrared-correlated 31-GHz radio emission from Orion East," *Monthly Notices of the Royal Astronomical Society*, vol. 407, pp. 2223–2229, 2010.

[129] T. L. Wilson and R. T. Rood, "Abundances in the interstellar medium," *Annual Review of Astronomy & Astrophysics*, vol. 32, no. 1, pp. 191–226, 1994.

[130] M. Vidal, S. Casassus, C. Dickinson et al., "Dust-correlated cm wavelength continuum emission from translucent clouds ζOph and LDN 1780," *Monthly Notices of the Royal Astronomical Society*, vol. 414, pp. 2424–2435, 2011.

[131] P. Castellanos, S. Casassus, C. Dickinson et al., "Dust-correlated centimetre-wave radiation from the M78 reflection nebula," *Monthly Notices of the Royal Astronomical Society*, vol. 411, no. 2, pp. 1137–1150, 2011.

[132] D. A. Green, "A revised Galactic supernova remnant catalogue," *Bulletin of the Astronomical Society of India*, vol. 37, pp. 45–61, 2009.

[133] W. T. Reach, J. Rho, A. Tappe et al., "A *Spitzer Space Telescope* Infrared Survey of supernova remnants in the inner Galaxy," *The Astronomical Journal*, vol. 131, no. 3, article 1479, 2006.

[134] S. Casassus, C. Dickinson, K. Cleary and et al., "Centimetre-wave continuum radiation from the ρ Ophiuchi molecular cloud," *Monthly Notices of the Royal Astronomical Society*, vol. 391, pp. 1075–1090, 2008.

[135] S. Casassus, L. Å. Nyman, C. Dickinson, and T. J. Pearson, "A centimetre-wave excess over free-free emission in planetary nebulae," *Monthly Notices of the Royal Astronomical Society*, vol. 382, no. 4, pp. 1607–1622, 2007.

[136] B. M. Pazderska, M. P. Gawroński, R. Feiler et al., "Survey of planetary nebulae at 30 GHz with OCRA-p," *Astronomy & Astrophysics*, vol. 498, pp. 463–470, 2009.

[137] G. Umana, P. Leto, C. Trigilio et al., "Millimeter observations of planetary nebulae," *Astronomy & Astrophysics*, vol. 482, no. 2, pp. 529–534, 2008.

[138] E. J. Murphy, G. Helou, J. J. Condon et al., "The detection of anomalous dust emission in the nearby galaxy ngc 6946," *The Astrophysical Journal Letters*, vol. 709, no. 2, article L108, 2010.

[139] T. Murphy, E. M. Sadler, R. D. Ekers et al., "The Australia Telescope 20 GHz Survey: the source catalogue," *Monthly Notices of the Royal Astronomical Society*, vol. 402, pp. 2403–2423., 2010.

[140] R. C. Kennicutt Jr., L. Armus, G. Bendo et al., "SINGS: The *SIRTF* Nearby Galaxies Survey," *Publications of the Astronomical Society of the Pacific*, vol. 115, pp. 928–952, 2003.

[141] F. Walter, E. Brinks, W. J. G. De Blok et al., "Things: the Hi nearby galaxy survay," *The Astronomical Journal*, vol. 136, no. 6, pp. 2563–2647, 2008.

[142] L. F. Rodriguez, "Radio observations of outflows," *Bulletin of the American Astronomical Society*, vol. 21, p. 786, 1989.

[143] G. Anglada, "Centimeter continuum emission from outflow sources," in *Revista Mexicana de Astronomia y Astrofisica Serie de Conferencias*, vol. 1, p. 67, 1995.

[144] P. Andre, T. Montmerle, and E. D. Feigelson, "A VLA survey of radio-emitting young stars in the Rho Ophiuchi dark cloud," *The Astronomical Journal*, vol. 93, pp. 1182–1198, 1987.

[145] D. Stamatellos, D. Ward-Thompson, A. P. Whitworth, and S. Bontemps, "A VLA search for young protostars embedded in dense cores," *Astronomy & Astrophysics*, vol. 462, no. 2, pp. 677–682, 2007.

[146] L. F. Rodriguez and J. Canto, "Stellar winds and molecular clouds—a search for ionized stellar winds," *Revista Mexicana De Astronomia Y Astrofisica*, vol. 8, no. 2, p. 163, 1983.

[147] J. H. Bieging, M. Cohen, and P. R. Schwartz, "VLA observations of T Tauri stars. II—a luminosity-limited survey of Taurus-Auriga," *The Astrophysical Journal*, vol. 282, pp. 699–708, 1984.

[148] S. H. Pravdo, L. F. Rodriguez, S. Curiel et al., " Detection of radio continuum emission from Herbig-Haro objects 1 and 2 and from their central exciting source," *The Astrophysical Journal*, vol. 293, pp. L35–L38, 1985.

[149] L. F. Rodriguez and B. Reipurth, "VLA detection of the exciting sources of HH 83, HH 117, HH 124, HH 192, HH 300, HH 366, and HH 375," *Revista Mexicana De Astronomia Y Astrofisica*, vol. 34, p. 13, 1998.

[150] P. Andre, F. Motte, and A. Bacmann, "Discovery of an extremely young accreting protostar in Taurus," *The Astrophysical Journal Letters*, vol. 513, no. 1, article L57, 1999.

[151] A. M. M. Scaife, J. Hatchell, M. Davies et al., "AMI-LA radio continuum observations of *Spitzer* c2d small clouds and cores: Perseus region," *Monthly Notices of the Royal Astronomical Society*, vol. 415, pp. 893–910, 2011.

[152] A. M. M. Scaife, E. I. Curtis, M. Davies et al., "AMI Large Array radio continuum observations of *Spitzer* c2d small clouds and cores," *Monthly Notices of the Royal Astronomical Society*, vol. 410, no. 4, pp. 2662–2678, 2011.

[153] A. M. M. Scaife, J. Hatchell, R. E. Ainsworth et al., "AMI-LA radio continuum observations of *Spitzer* c2d small clouds and cores: Serpens region," *Monthly Notices of the Royal Astronomical Society*, vol. 420, pp. 1019–1033, 2012.

[154] S. Curiel, L. F. Rodriguez, J. Bohigas, M. Roth, J. Canto, and J. M. Torrelles, "Extended radio continuum emission associated with V645 CYG and MWC1080," *Astrophysical Letters and Communications*, vol. 27, pp. 299–309, 1989.

[155] K. H. A. Winkler and M. J. Newman, "Formation of solar-type stars in spherical symmetry. I—the key role of the accretion shock," *The Astrophysical Journal*, vol. 236, pp. 201–211, 1980.

[156] P. Cassen and A. Moosman, "On the formation of protostellar disks," *Icarus*, vol. 48, no. 3, pp. 353–376, 1981.

[157] S. Curiel, J. Canto, and L. F. Rodriguez, "A model for the thermal radio continuum emission produced by a shock wave and its application to the Herbig-Haro objects 1 and 2," *Revista Mexicana de Astronomia y Astrofisica*, vol. 14, pp. 595–602, 1987.

[158] L. F. Rodriguez and B. Reipurth, "VLA detection of the exciting sources of HH 34, HH 114, and HH 199," *Revista Mexicana De Astronomia Y Astrofisica*, vol. 32, pp. 27–33, 1996.

[159] G. Anglada, "Radio Jets in young stellar objects," in *Astronomical Society of the Pacific Conference Series (ASPC '96)*, vol. 93, University of Barcelona, Barcelona, Spain, July 1996.

[160] G. Anglada, E. Villuendas, R. Estalella et al., "Spectral indices of centimeter continuum sources in star-forming regions: implications on the nature of the outflow exciting sources," *Astronomical Journal*, vol. 116, no. 6, pp. 2953–2964, 1998.

[161] M. Simon, M. Felli, L. Cassar, J. Fischer, and M. Massi, "Infrared line and radio continuum emission of circumstellar ionized regions," *The Astrophysical Journal*, vol. 266, pp. 623–645, 1983.

[162] T. L. Bourke, A. Crapsi, P. C. Myers et al., "Discovery of a low-mass bipolar molecular outflow from L1014-IRS with the submillimeter array," *The Astrophysical Journal Letters*, vol. 633, no. 2, article L129, 2005.

[163] A. Crapsi, C. H. DeVries, T. L. Huard et al., "Dynamical and chemical properties of the "starless" core L1014," *Astronomy & Astrophysics*, vol. 439, pp. 1023–1032, 2005.

[164] A. Scaife, "Radio Emission from Young Stellar Objects," *AstRv*, vol. 7, Article ID 040000, 2012.

[165] M. M. Dunham and E. I. Vorobyov, "Resolving the luminosity problem in low-mass star formation," *The Astrophysical Journal*, vol. 747, no. 1, article 52, 2012.

[166] A. G. G. Tielens M, S. Hony, C. van Kerckhoven, and E. Peeters, "Interstellar and circumstellar PAHs," ESA-SP 427, 579, 1999.

[167] A. G. G. Tielens M, "Interstellar polycyclic aromatic hydrocarbon molecules," *Annual Review of Astronomy & Astrophysics*, vol. 46, pp. 289–337, 2008.

[168] E. Peeters, H. W. W. Spoon, and A. G. G. M. Tielens, "Polycyclic aromatic hydrocarbons as a tracer of star formation?" *The Astrophysical Journal*, vol. 613, no. 2, pp. 986–1003, 2004.

[169] A. P. Jones, A. G. G. M. Tielens, and D. J. Hollenbach, "Grain shattering in shocks: the interstellar grain size distribution," *Astrophysical Journal Letters*, vol. 469, no. 2, pp. 740–764, 1996.

[170] B. T. Draine, "Photoelectric heating of interstellar gas," *The Astrophysical Journal*, vol. 36, pp. 595–619, 1978.

[171] H. J. Habing, "The interstellar radiation density between 912 A and 2400 A," *Bulletin of the Astronomical Institutes of the Netherlands*, vol. 19, p. 421, 1968.

[172] N. Ysard and L. Verstraete, "The long-wavelength emission of interstellar PAHs: characterizing the spinning dust contribution," *Astronomy & Astrophysics*, vol. 509, article A12, 2010.

[173] B. T. Draine and A. Li, "Infrared emission from interstellar dust. IV. The Silicate-Graphite-PAH Model in the Post-*Spitzer* Era," *The Astrophysical Journal*, vol. 657, no. 2, article 810, 2007.

[174] S. Casassus, A. C. S. Readhead, T. J. Pearson, L. Å. Nyman, M. C. Shepherd, and L. Bronfman, "Anomalous radio emission from dust in the Helix," *The Astrophysical Journal*, vol. 603, no. 2, pp. 599–610, 2004.

[175] J. W. M. Baars, R. Genzel, I. I. K. Pauliny-Toth, and A. Witzel, "The absolute spectrum of CAS A—an accurate flux density scale and a set of secondary calibrators," *Astronomy & Astrophysics*, vol. 61, no. 1, pp. 99–106, 1977.

[176] N. Rees, "Comments on the absolute flux density scale at low radio frequencies," *Monthly Notices of the Royal Astronomical Society*, vol. 243, pp. 637–639, 1990.

[177] Y. A. Hafez, R. D. Davies, R. J. Davis et al., "Radio source calibration for the very small array and other cosmic microwave background instruments at around 30 GHz," *Monthly Notices of the Royal Astronomical Society*, vol. 388, no. 4, pp. 1775–1786, 2008.

[178] J. L. Weiland, N. Odegard, R. S. Hill et al., "seven-year *wilkinson microwave anisotropy probe* (*wmap* ∗) observations: planets and celestial calibration sources," *The Astrophysical Journal*, vol. 192, no. 2, article 19, 2011.

[179] D. J. Rudy, D. O. Muhleman, and G. L. Berge, "Mapping of the 2 and 6cm thermal emission from mars using the very large array," *Bulletin of the American Astronomical Society*, vol. 19, p. 834, 1987.

[180] D. Johnstone, J. Di Francesco, B. Matthews et al., "The science case for building a band 1 receiver suite for ALMA," http://arxiv.org/abs/0910.1609.

[181] B. Acke and M. E. Van Den Ancker, "ISO spectroscopy of disks around Herbig Ae/Be stars," *Astronomy & Astrophysics*, vol. 426, no. 1, pp. 151–170, 2004.

[182] R. R. Rafikov, "Microwave emission from spinning dust in circumstellar disks," *The Astrophysical Journal*, vol. 646, pp. 288–296, 2006.

[183] C. R. Purcell, M. G. Hoare, and P. Diamond, "The CORNISH Survey of the galactic plane," in *Astronomical 2008 Society of the Pacific Conference Series (ASPC '08)*, vol. 387, p. 389, 2008.

[184] M. Thompson, S. Goedhart et al., The MeerKAT Galactic Plane Survey (MeerGAL), http://star.herts.ac.uk/progs/surveys_mw_radio.html.

[185] Y. Perrott, A. M. M. Scaife, D. A. Green et al., "AMI Galactic Plane Survey at 16 GHz: I. Observing, mapping and source extraction," *Monthly Notices of the Royal Astronomical Society*, 2013.

[186] I. Bains, M. Cohen, J. M. Chapman, R. M. Deacon, and M. P. Redman, "Revealing the transition from post-AGB stars to planetary nebulae: non-thermal and thermal radio continuum observations," *Monthly Notices of the Royal Astronomical Society*, vol. 397, no. 3, pp. 1386–1401, 2009.

[187] E. M. Waldram, G. G. Pooley, K. J. B. Grainge et al., "9C: a survey of radio sources at 15 GHz with the Ryle Telescope," *Monthly Notices of the Royal Astronomical Society*, vol. 342, no. 3, pp. 915–925, 2003.

[188] R. S. Furuya, Y. Kitamura, A. Wootten, M. J. Claussen, and R. Kawabe, "Water maser survey toward low-mass young stellar objects in the northern sky with the Nobeyama 45 meter telescope and the very large array," *The Astrophysical Journal Supplement Series*, vol. 144, no. 1, pp. 71–134, 2003.

[189] C. T. Tibbs, A. M. M. Scaife, C. Dickinson et al., "AMI observations of the anomalous microwave emission in the perseus molecular cloud," http://arxiv.org/abs/1303.5501.